EUROPEAN ORGANIZATION FOR NUCLEAR RESEARCH
CERN – SL DIVISION

CERN-SL-2002-060 ECT

Transient Thermo-Mechanical Analysis of the TPSG4 Beam Diluter

B. Goddard, R. Guinand, A. Herrera-Martínez, Y. Kadi, S. Marque

Abstract

A new extraction channel is being built in the Super Proton Synchrotron (SPS) Long Straight Section 4 (LSS4) to transfer proton beams to the Large Hadron Collider (LHC) and also to the CERN Neutrino to Gran Sasso (CNGS) target. The beam is extracted in a fast mode during a single turn. For this purpose a protection of the MSE copper septum coil, in the form of a beam diluting element placed upstream, will be required to cope with the new failure modes associated with the fast extraction operation. The present analysis focuses on the thermo-mechanical behavior of the proposed TPSG4 diluter element irradiated by a fast extracted beam (up to 4.9 x 10^{13} protons per 7.2 μs pulse) from the SPS. The deposited energy densities, estimated from primary and secondary particle simulations using the high-energy particle transport code FLUKA, were converted to internal heat generation rates taken as a thermal load input for the finite-element engineering analyses code ANSYS. According to the time dependence of the extracted beam, the transient solutions were obtained for coupled heat transfer, structural deformation, and shock wave problems. The results are given for the space distribution and the time evolution of temperatures and stresses in the most critical parts of the TPSG4 beam diluting element followed by the MSE copper septum coil. In the worst case of impact of the full LHC ultimate beam, the maximum temperatures remain safely below the melting point. However, the maximum equivalent stresses may slightly exceed the elastic limit in the aluminium section of the diluter. Also, the predicted maximum temperature rise in the MSE septum coil exceeds the design value.

Geneva, Switzerland
December, 2002

Table of Content

List of Figures

List of Tables

1 Introduction

A new extraction channel [1] is being built in the Super Proton Synchrotron (SPS) Long Straight Section 4 (LSS4) to transfer proton beams to the Large Hadron Collider (LHC) and also to the CERN Neutrino to Gran Sasso (CNGS) target. The beam is extracted in a fast mode during a single turn. A "slow" closed orbit bump is applied to move the entire beam close to the septum, and then the MKE extraction kicker fires to deflect the entire beam across an extraction septum in what should be a loss-free process (for CNGS the beam is extracted in two parts using the same principle). The extraction channel must be able to accept the high brightness LHC proton beam at *450 GeV/c*, and also the high intensity, large emittance fixed target CNGS proton beam at *400 GeV/c*. In this respect, the extraction system should be adequately protected against mis-steered beams.

The present analysis focuses on the thermo-mechanical behavior of the proposed TPSG4 protection element irradiated by a fast extracted beam (up to 4.9×10^{13} protons per $7.2\ \mu s$ pulse at *450 GeV/c* extraction momentum) from the SPS. The deposited energy densities, estimated from primary and secondary particle simulations using the high-energy particle transport code FLUKA [2], are converted to internal heat generation rates taken as a thermal load input for the finite-element engineering analyses code ANSYS [3]. According to the time dependence of the extracted beam, the transient solutions are obtained for coupled heat transfer, structural deformation, and shock wave problems. The results are given for the space distribution and the time evolution of temperatures and stresses in the most critical parts of the TPSG4 protection element and downstream MSE copper septum coil.

2 Septum Protection Requirements

Direct impact of the extracted beam would destroy the copper septum magnet coils [4,5]. A comprehensive interlock system will be required to survey the beam positions, losses, bumper and septum currents, kicker charging voltages, etc. However, failure modes resulting in impact of the beam on the septum coil are nevertheless possible [6]. A physical protection element (diluter) will therefore be required.

2.1 TPSG4 Concept

The TPSG4 is an element designed to dilute the proton beam sufficiently to protect the copper coils of the MSE septum magnet from damage in the event of mis-steered beams at extraction [6]. The TPSG4 element is located in the extraction channel, immediately after the lattice quadrupole QFA418, and just before the extraction septum, as illustrated in Figure 1. It should reduce the particle flux on the copper coils of the septum magnet to a safe level, such that the temperature does not exceed the chosen target value of *100 ºC*.

The TPSG4 diluter element geometry is essentially defined by the trajectories of the extracted beam, the width of the MSE septum coil (*17.25 mm*) plus the alignment tolerances, and the height of the MSE magnet gap (*20 mm*). A diluter element section of $19.25 \times 20\ mm^2$ has been decided (Figure 2). The limited available space imposes restrictions on the total length available for the TPSG4 diluter element (a maximum of *3.25 m*).

Previous work [4] showed that a diluter element comprising *2.35 m* of carbon (density $1.77\ g/cm^3$) followed by *0.9 m* of aluminium (density $2.699\ g/cm^3$) would suffice to keep the

temperature of the copper coil below *100 ºC* in the case of the full LHC ultimate beam at normal incidence.

The TPSG4 diluter element will be supported in a rigid frame (yoke). For reasons of radioprotection, in order to maximise the shielding effect as close to the source as possible, this yoke will be made of steel and will have approximately the same section as the magnetic yokes of the MSE septum magnets (Figure 3). For reasons of machine impedance, the TPSG4 must contain a beam screen (Figure 4), similar to that developed for the MSE septum magnets. For vacuum reasons the TPSG4 tank will have vacuum pumps directly attached, and the assembly must also be bakeable.

2.2 Beam Characteristics

For the purpose of the analysis, the LHC ultimate beam is considered as the worst case, since the low emittance and high intensity result in a very high spatial proton density on the beam axis. The relevant nominal beam parameters are summarised in Table 1.

The layout of the LSS4 extraction channel has been optimised to maximise the aperture available for the injected, circulating and extracted beams. Figure 5 shows the horizontal trajectories through the LSS4 extraction for the LHC beam at injection and during extraction.

Two failure modes for investigation are postulated:

1. **Worst case**, where the settings are such that the entire LHC **ultimate beam** is dumped into the septum;
2. **MKE sweep**, where the kicker timing is wrong such that the LHC **nominal beam** is swept across the septum.

A thermo-mechanical analysis is required to validate the conceptual design of the TPSG4 diluter element for use in LSS4 which: (i) **MUST** protect the MSE septum against failure mode 2; and **SHOULD** protect the MSE septum against failure mode 1, given the constraints.

3 Energy Deposition Calculations

3.1 Simulation of the Particle Cascades

The primary and secondary cascades induced by the LHC beam in the TPSG4 diluter element were simulated using the FLUKA-2001 version 2.0 high-energy particle transport code [2]. Comparisons with measurements of absorbed dose distribution around the SPS beam [7] had shown that an accuracy of better that *25%* could be expected when estimating the densities of deposited energy from Monte Carlo calculations with this code. A summary of the parameters assumed for the current study is given in Table 1.

The model for analysis [8] consists of a rod having a total length of *325 cm* and a cross-section of *1.6 x 2.0 cm*^{2}. The first *235 cm* is made of carbon followed by *90 cm* of aluminium. The whole structure is surrounded by an iron yoke (outer dimensions: *25.6 x 25.2 cm*^{2}) in order to reduce the stray radiation. The structure of the diluter element can be seen in Figure 1. The element is axially irradiated by a *450 GeV/c* mono-energetic proton beam which horizontal and vertical profiles are taken to be Gaussian *(σ_H = 0.95 mm; σ_V = 0.4 mm*).

The interactions, transport and energy deposition processes were followed down to the kinetic energy threshold of *100 keV* for all charged particles (hadrons, muons and electrons), down to *10 keV* for photons, and down to *0.4 eV* for neutrons (FLUKA default card: PRECISION). Particles slowed down or produced with energies below these thresholds were assumed to deposit their energy locally. The energy lost by charged particles in ionization processes, was converted to emitted δ-rays (low energy electrons), and thus further distributed around ionizing particle tracks. Only neutrinos and anti-neutrinos were discarded.

Multiple Coulomb scattering was included down to Molliere's theory limit, for the primaries and secondaries. Electron pair production and bremsstrahlung photon emission were taken into account also for hadrons and muons. Relatively rare processes of the electro- and photo-production of hadrons were neglected. None of the biasing or importance sampling methods available in FLUKA was used.

3.2 Estimation of Deposited Energy Densities

3.2.1 Worst Case: entire LHC ultimate beam dumped into the TPSG4 diluter

Non symmetrical *(x,y,z)* cartesian binning meshes with *100* vertical steps of $\Delta x=0.02$ *cm*, *50* horizontal steps of $\Delta y=0.032$ *cm* and *325* longitudinal steps of $\Delta z=1.0$ *cm* were applied to score the density of energy deposited in the TPSG4 diluter element and in the subsequent MSE septum copper coil.

Figure 6 shows the maximum value of the energy density deposited along the length of the TPSG4 diluter element and of the first part of the MSE coil. The results show that the first metre of the graphite section as the most critical one: the local concentration of deposited energy reaches the maximum value of $0.27 \pm 5\%$ *GeV/cm*^{3} per primary proton at about *21 cm* depth in the graphite rod. Moreover, the longitudinal and radial gradient of energy deposition is steepest for the first *15 cm*, thus the maximum temperatures and resultant thermal stresses have to be expected in this section, even though the total energy deposited in graphite amounts to only *25.5 GeV/p* (i.e. *5.5%* of the total incident proton energy). Similarly, the local concentration of deposited energy reaches a maximum value of $0.1 \pm 10\%$ *GeV/cm*^{3} per primary proton at about *10 cm* depth in the aluminium rod and $0.06 \pm 20\%$ *GeV/cm*^{3} per primary proton at about *5 cm* depth in the copper coil even though the total energy deposited in these sections amount to *7* and *9 GeV/p* respectively (i.e. *1.6* and *2%* of the total incident proton energy respectively). *160 GeV/p* is deposited in the yoke of the diluter element (*36%*), and the rest of the energy (*54.9%*) is deposited outside by particles escaping the system.

Figure 7 shows a first calculation of the instantaneous temperature profile along the length of the TPSG4 diluter element and of the first part of the MSE coil, based on the estimation of the maximum value of the energy density deposition. In practice, a small amount of energy density dE deposited in a volume dV of a material with density ρ causes a temperature rise ΔT determined by $dE = c_p \rho dV \Delta T$. The proportionality constant c_p is the specific heat of the considered material. The larger the value of c_p, the smaller the temperature rise caused by an energy deposit dE. For important energy deposition the specific heat can no longer be considered as constant, but its temperature dependence must be taken into account. The specific heat $c_p(T)$ for graphite is shown in Table 2 (for iron, copper and aluminium the heat capacity is assumed to be constant over the expected range of temperature).

Now ΔT must be extracted from:

$$\frac{dE}{dV} = \rho \int_{T_0}^{T_0 + \Delta T} c_p\,(T) dT$$

by solving numerically for the upper limit of the integral. The material temperature before the beam impact is T_0. A more correct and detailed non-linear transient thermal analysis of the TPSG4 diluter element is described in Section 4.

As expected, the temperature observed in the graphite section of the diluter rises steeply during the first *15 cm* up to a maximum value of about *825 ºC* (i.e. well below the melting point of carbon ≈ *3550 ºC*), and then decreases slowly down to about *235 ºC* at the depth of *2.35 m*. At that depth a strong increase of the temperature, up to a value of *285 ºC* can be observed. This can be explained by the change of materials (from carbon to aluminium) inside the diluter. In general two facts influence the behaviour of the temperature rise inside irradiated matter. The first can be found in the individual stopping power of a material (E_{dep}/cm^3) and the second is given by the product of the specific heat capacity with the density of the material. In this particular case the stopping power of aluminium is higher than the one of carbon, whereas the product of density and specific heat capacity is about the same for both materials within the expected temperature range. The same effect can be observed when the beam enters the first part of the MSE magnet (copper), where the temperature inside the coil rises to a maximum value of about *165 ºC*, which is higher than the *100 ºC* aimed for.

3.2.2 MKE Sweep: LHC nominal beam is swept across the TPSG4 diluter

As in the previous case, non symmetrical *(x,y,z)* cartesian binning meshes with *150* vertical steps of *Δx=0.02 cm*, *50* horizontal steps of *Δy=0.0385 cm* and *290* longitudinal steps of *Δz=1.0 cm* were applied to score the density of energy deposited in the TPSG4 diluter element and in the subsequent MSE septum copper coil.

The model for analysis has evolved with respect to the previous case and consists of a rod having a total length of *290 cm* (instead of *325 cm*) and a cross-section of *1.925 x 3.0 cm^2* (instead of *1.6 x 2.0 cm^2*). The first *210 cm* is made of carbon followed by *80 cm* of aluminium. The whole structure is surrounded by an iron yoke (outer dimensions unchanged: *25.6 x 25.2 cm^2*) in order to reduce the stray radiation. The element is axially irradiated by a *450 GeV/c* mono-energetic proton beam which horizontal and vertical profiles are taken to be Gaussian *(σ_H = 0.97 mm* instead of *0.95 mm* previously*; σ_V = 0.4 mm* unchanged).

Figure 8 shows the maximum value of the energy density deposited along the length of the TPSG4 diluter element after being irradiated at the centre and on both sides, in order to account for the boundary effects when simulating the beam sweeping. The results obtained are very similar to those calculated in the worst case: the local concentration of deposited energy reaches the maximum value of *0.26 ± 4% GeV/cm^3* per primary proton at about *20 cm* depth in graphite for the beam hitting at the centre, and between *0.21* and *0.24 ± 5.5% GeV/cm^3* per primary proton for the beam hitting the sides of the diluter.

Similarly, the local concentration of deposited energy reaches a maximum value of *0.13 ± 12% GeV/cm^3* per primary proton at about *13 cm* depth in aluminium for the beam hitting at the centre, and between *0.07* and *0.08 ± 15% GeV/cm^3* per primary proton for the beam hitting the sides of the diluter.

A detailed non-linear transient thermal analysis for this case is described in Section 4.

4 Transient thermo-mechanical analysis of TPSG4 beam diluter

4.1 Worst Case: entire LHC ultimate beam dumped into the diluter

The graphite and copper rods of the TPSG4 were subjected to a non-linear transient thermo-mechanical analysis, performed with the finite element package ANSYS [3].

4.1.1 Generation of the solid FE model

Due to the spatial distribution of energy deposition, the rods have been modelled in 3 dimensions. The model accounts for thermal and structural displacements degrees of freedom, allowing a direct coupled-field resolution of the problem. Taking into account the dynamics of the problem (energy deposition in *7.2* μs) and to reduce as far as possible numerical instabilities due to implicit codes, cubic first-order element have been selected. The corresponding element type in the ANSYS™ library is SOLID5: an eight node, first-order, coupled field solid.

Each rod has an element length, in the direction of the beam, of *10 mm*, to be consistent with the mesh used in FLUKA post processing. This leads to *235* and *90* element divisions (along beam axis) for the graphite and aluminium rod respectively.

The cross section of the rods is *20 mm* (height) by *16 mm* (width), the centre area (*1 mm* by *1.6 mm*) is meshed as the FLUKA user bin: *0.2 mm* by *0.32 mm* leading to *25* elements in this region. The remaining part of the cross section is meshed with *120* elements, thus the cross section contains *145* elements. The graphite rod is modelled by *34075* elements and the aluminium one by *13050* elements. The element contours, for a cross section, is illustrated in Figure 9.

4.1.2 Boundary conditions

A uniform temperature of *20 ºC* has been applied to start the analysis. Neither convection nor radiation was taken into account. Conduction could only take place inside each rod.

Both rods were applied fixed longitudinal displacements at both ends, fixed vertical displacements on the surfaces in contact with the yoke and fixed lateral displacements on the outer lateral face.

4.1.3 Material properties

Graphite and aluminium material properties at *20 ºC* are given in Table 2, the temperature-dependent ones are shown on Figure 10 a and b respectively; these data are as compiled in Ref. [9].

4.1.4 Loads

The spatial energy density deposition given by FLUKA is directly imported into the ANSYS mesh using a “map” operation. Energy density is applied as nodal heat generation rates. On one node in the ANSYS mesh is applied the heat generation rate resulting from a 3-D linear interpolation of the energy density of the neighbouring nodes in FLUKA.

The beams delivers its energy over a period of *7.2 μs*, thus the energy density expressed in J/m^3 has to be scaled by *2÷7.2 μs* to be applied as heat generation rate (*W/m^3*) into the finite element model. Assuming that the energy is linearly ramped from *0* to its maximum over that period.

The analysis considers only one dilution of the mis-steered beam, impacting totally in the centre of the cross section.

4.1.5 Load steps

Due to the dynamics of the loading, shock waves are of interest. In order to get an estimation of the dynamic stresses (even if the use of an implicit code is not the best solution), the time steps should be of the order of the traversal time of a shock wave to the closet boundary [7], i.e. *8 mm*. The sound velocity in graphite is about *2.4 km/s*, thus an elastic wave requires a time of *3 μs*, this is the maximum time step required to catch the evaluation of radial elastic waves (*964 μs* for longitudinal elastic waves).

A few first radial waves were observed over the period: *7.3 μs* to *57.3 μs* with a time resolution of *1 μs*. Then a few longitudinal waves were observed from *57.3 μs* to *5057.3 μs* with a time resolution of *100 μs*.

4.1.6 Results

Table 3 summarises the results of temperatures and stresses induced in both graphite and aluminium rods.

Temperature distribution and evolution

The temperature data are given for both rods at the end of the pulse and at *1 s*, for the entrance section, the maximum energy density section, the middle section and the exit section.

The maximum energy density is located at *+0.21 m* and *+0.11 m* from entrance face for graphite and aluminium rod respectively.

The temperature rise in graphite would be *+802 K* and *+250 K* in aluminium.

The time evolution of the on-axis temperatures, for the 4 latter sections, in both rods, is shown in Figure 11 (a: graphite and b: aluminium).

The 2-dimensional (cross section perpendicular to beam axis) temperature distribution at the end of pulse, in the section of maximum energy density is plotted in Figure 12 (a: graphite and b: aluminium).

The on-axis temperature distributions, at the end of the pulse, for both rods, are plotted in Figure 13 (a: graphite and b: aluminium). A temperature plot, in a longitudinal section, is shown in Figure 14 (a: graphite and b: aluminium). The height of each rod has been magnified for visualisation purpose.

Stress distribution and evolution

Due to the dynamics and the intensity of loading, the rods are subjected to high elastic pressure waves as described in Ref [10]. Table 3 tabulates, for both rods, the 3 principal (S1,

S2, S3) stresses (peak and dynamic) their corresponding equivalent stresses (Von Mises and Stassi criteria) and their vibration period. It should be noted that the use of an implicit scheme to solve non-linear dynamics problems is not the best (but the only available at the time at CERN) and leads to numerical instabilities.

Considering the geometry and loading, the principal stresses are oriented as following: S3 is along beam axis (X), S1 and S2 perpendicular to beam axis, S1 along Y-axis (width of the rods) and S2 along Z-axis (height of the rods).

- *Graphite rod:*

  Without material damping: the graphite rod is subjected to a compressive stress state characterized by a peak Stassi equivalent stress of *16 MPa* (which is *50%* of the tensile yield stress of a standard graphite). Shock waves are described by a transversal component (S1) at *27 μs* period (maximum amplitude *50 MPa*) and a longitudinal component (S3) at *2 ms* period (maximum amplitude *26 MPa*).

  With material damping: with damping ratio of 10^{-2} at 10^{5} *Hz* to 10^{-4} at 10^{3} *Hz*, the transversal shock waves are damped. The longitudinal component is left unchanged. The peak Stassi equivalent stress is reduced to *4 MPa*.

- *Aluminium rod:*

  Without material damping: The graphite rod is mainly subjected to a compressive stress state although S1 oscillates between tensile and compressive stresses. The peak Von Mises equivalent stress is *684 MPa*, reached in the *10 μs* time scale, which is *25%* higher than the maximum tensile yield stress of an AA-7000 series. The components of the shock waves are *11 μs* period on S1 direction (maximum amplitude *640 MPa*) and *0.4 ms* period on S3 direction (maximum amplitude *520 MPa*).

  With material damping: With damping ratio of 10^{-2} at 10^{5} *Hz* to 10^{-4} at 10^{3} *Hz*, the transversal shock waves are hardly damped. The longitudinal component is left unchanged. The peak Von Mises equivalent stress is reduced to *360 MPa*, an AA-7000 series alloy should withstand these stresses.

Figures

The time evolution of the three principal stresses (S1, S2 and S3) at point of maximum energy density, in both rods, is plotted in Figure 15 (a: graphite and b: aluminium).

The principal stresses along beam axis (in graphite and aluminium rods) at the end of the pulse are plotted in Figure 16 (a: graphite and b: aluminium).

Distribution of the principal stresses in the maximum energy density cross section at the end of pulse, is plotted in Figure 17 (a: graphite and b: aluminium).

4.2 MKE Sweep: LHC ultimate beam is swept across the septum.

The graphite and copper rods of the TPSG4 were subjected to a non-linear transient thermo-mechanical analysis, performed with the finite element package ANSYS [3].

4.2.1 Generation of the solid FE model

Due to the complicated structure for the loading and to allow for quicker evaluation of the behaviour of the diluter, the rods have been modelled in 2 dimensions, in the plane containing the centre of the bunches. Although this model is not theoretically correct, the loading cannot be considered constant in the direction perpendicular to the plane modelled. Similar 2D calculations performed on the previous model (worst case) showed that results are in good agreement with those of a 3D calculation in the region where the heat load is applied. The model accounts for thermal and structural displacements degrees of freedom, allowing a direct coupled-field resolution of the problem. The element type used in the ANSYS library is plane13: a four node, first-order, coupled field solid. Calculations were made with the "plane strain" option.

To be able to evaluate the elastic waves, the mesh should fulfil the following requirement: "*20* elements on the shorter wavelength of interest". In our case, we have evaluated the first longitudinal and transversal resonance frequency for each rod. Taking into account an average sound speed of *2400 m/s* for the carbon and *5100 m/s* for the aluminium this leads to the following figures:

	Longitudinal element edge length (mm)	**Transversal element edge length (mm)**
Carbon rod	720	7.2
Aluminium rod	153	3

The physical length of each rod has been reduced in this second analysis from *2.35 m* to *2.10 m* for the graphite rod and from *0.9 m* to *0.8 m* for the aluminium one. The cross section of the rods has also evolved from *20 mm* (height) to *30 mm* and from *16 mm* (width) to *19.25 mm.*

Each rod has an element length, in the direction of the beam (longitudinal direction), of *10 mm*, to be consistent with the mesh used in FLUKA post processing. This leads to *210* and *80* element divisions (along beam axis) for the graphite and aluminium rod respectively. There are *50* elements on the width of the rods as used in the FLUKA post processing, leading to *0.385 mm* element edge length, which is compliant with the above numerical requirements. The graphite rod is modelled by *10500* elements and the aluminium one by *4000* elements. The element contours are illustrated in Figure 18.

4.2.2 Boundary conditions

A uniform temperature of *20 ºC* has been applied to start the analysis. Neither convection nor radiation was taken into account. Conduction could only take place inside each rod and at the interface between the 2 rods.

Both rods were applied fixed longitudinal displacements at both ends and fixed displacements on the lateral faces.

4.2.3 Material properties

Graphite and aluminium material properties at *20 ºC* are given in Table 2, the temperature-dependent ones are shown on Figure 10 a and b respectively; these data are as compiled in Ref. [9].

4.2.4 Loads

The spatial energy density deposition given by FLUKA is directly imported into the ANSYS mesh using a "map" operation. Energy density is applied as nodal heat generation rates. On one node in the ANSYS mesh is applied the heat generation rate resulting from a 2D linear interpolation of the energy density of the neighbouring nodes in FLUKA.

The analysis considers *21* bunches hitting the diluter, with a bunch spacing of *25 ns*. The horizontal bunch separation on the entrance face of the diluter is *0.93 mm*.

We supposed that a bunch lasts for *1ns*, thus the energy density expressed in J/m^3 has to be scaled by *2÷1 ns* to be applied as heat generation rate (W/m^3) into the finite element model. Assuming that the energy is linearly ramped from *0* to its maximum value over that period.

4.2.5 Load steps

Each individual bunch has been represented by a load step (*1 ns*, linearly ramped), followed by a *24 ns* load step representing the bunch spacing. Thus, the overall loading lasts for *501 ns* and is represented by *41* load steps (*1* sub-step for each load step).

Afterwards, the following scheme has been used to track the behaviour of the rods, particularly the elastic shock waves in the ms time scale and the temperature evolution in the minute time scale:

Load Step	Number of sub steps (duration)	Time at end of load step
42 (unloading)	1 (1 ns)	502 ns
43	100 (500 ns)	50.502 μs
44	100 (50 μs)	5.05 ms
45	100 (250 μs)	30.05 ms
46	100 (500 μs)	80.05 ms
47	10 (92 ms)	1 s
48	10 (11.9 s)	2 min.
49	10 (88 s)	16 min 40 s
50	10 (900 s)	2 h 46 min 40 s

4.2.6 Results

Table 4 summarises the results of temperatures and stresses induced in both graphite and aluminium rods.

Temperature distribution and evolution

The temperature data are given for both rods at the end of the sweep and at *10000 s*, for the entrance section (*X=0*), the maximum thermal load section (*X=max(J)*) and the exit section (*X=l*).

The maximum thermal load section is located at *+1.18 m* and *+0.10 m* from entrance face for graphite and aluminium rod respectively.

The temperature rise in graphite would be *+36 K* and *+21 K* in aluminium after the beam is completely swept across the absorber.

The time evolution of the on-axis temperatures, for the 3 latter sections, in both rods, is shown in Figure 19 (a graphite and b aluminium).

The on-axis temperature distributions, at the end of the sweep, for both rods is plotted in Figure 20 a. A 2D temperature plot is shown in Figure 20 b. The height of each rod has been magnified for visualisation purpose.

Stress distribution and evolution

Table 4 tabulates, for both rods, the 3 principal (S1, S2, S3) stresses (peak and dynamic), their corresponding equivalent stresses (Von Mises and Stassi criteria) and their vibration period.

Considering the geometry and loading, the principal stresses are oriented as following: S1 is along beam axis (X), S2 and S3 perpendicular to beam axis, S2 along Y-axis (width of the rods) and S3 along Z-axis (height of the rods).

- *Graphite rod:*

  Without material damping: The graphite rod is subjected to a compressive stress state. The peak Stassi equivalent stress is *~ 0 MPa* which, obviously, is acceptable.
  Shock waves exhibit a transversal component of *10 μs* period and *1 MPa* of maximum amplitude and a longitudinal component (period *1.8 ms*) of *0.8 MPa* maximum amplitude.
  With material damping: With damping ratio of 10^{-2} at 10^{5} *Hz* to 10^{-4} at 10^{3} *Hz*, The amplitude of the transversal shock waves is reduced by *20%*. The peak Stassi equivalent stress is always negligible.

- Aluminium rod:

  Without material damping: The aluminium rod is subjected to a compressive stress state. The peak Von Mises equivalent stress is *21 MPa*, far below whatever aluminium alloy tensile yield strength. Shock waves are characterized by a transversal component at *3.4 μs* period and *35 MPa* of maximum amplitude and by a longitudinal component of *0.25 ms* period and *42 MPa* of maximum amplitude.

  With material damping: With damping ratio of 10^{-2} at 10^{5} *Hz* to 10^{-4} at 10^{3} *Hz*, The amplitude of the transversal shock waves is reduced by *35%* and by *15%* for the

longitudinal component (Maximum values on principal stresses). The peak Von Mises equivalent stress is not significantly changed.

Figures:

The time evolution of the three principal stresses (S1, S2 and S3) at the point of maximum thermal load, in both rods, is plotted in Figure 21 (a: graphite and b: aluminium).

The principal stresses along beam axis (in graphite and aluminium rods) at the end of the steps are plotted in Figure 22 (a: graphite and b: aluminium).

Distribution of the principal stresses in the maximum thermal load cross section at the end of the sweep, is plotted in Figure 23 (a: graphite and b: aluminium).

Details of elastic waves, without and with material damping, are reported respectively in Figure 24 (a and b) for graphite and for aluminium in Figure 25 (a and b).

5 Conclusions

In the case of an entire LHC ultimate beam dumped straight into the TPSG4 diluter element (worst case), the graphite and aluminium rods were subjected to a 3-D coupled particle cascade, transient non-linear thermo-mechanical analyses. The temperature increase in each rod, $\Delta T = +802\ K$ (graphite) and $+250\ K$ (aluminium), should not be an issue. The Stassi equivalent stresses in the graphite rod are always far below the tensile yield stress of a standard graphite (with or without material damping). For the aluminium rod and in the case of no material damping, the maximum Von Mises equivalent stress is *25%* above the tensile yield stress of an AA-7000 series aluminium alloy. With material damping (damping ratio of common values), the peak Von Mises equivalent stress is reduced to *65%* of the tensile yield stress of an AA-7150 aluminium alloy. In all cases, displacement restraints on all faces should be applied to both rods to decrease further the equivalent stresses.

The surrounding yoke, consisting of iron, which is meant to provide supplementary shielding, should also survive the predicted temperature rise, which closest to the diluter, should not exceed $+155\ K$ in the worst case. This value decreases rapidly with increasing depth in the C and Al rods.

The predicted maximum temperature rise in the MSE septum coil, $+145\ K$, exceeds by more than *80%* the target value, such that the simulated solid copper coil is locally heated to about $165\ ^oC$. However, the real coil contains cooling channels through which cooling water flows at a rate of about *1.2 litre / second*, with a minimum pressure of about *8 bar*. The high pressure and flow rate, together with the high heat capacity and enthalpy of water, mean that a local temperature rise in the copper to $165\ ^oC$, although undesirable, should not pose a problem for the septum, even for the worst case assumption of full beam loss at LHC ultimate intensity. Nevertheless, if further analysis shows that an improvement can be gained by altering the materials used, an upgrade of the TPSG4 could be possible at a later stage.

In the case of an entire LHC nominal beam swept across the TPSG4 diluter element, the graphite and aluminium rods were also subject of a coupled 3-D particle cascade, 2-D transient non-linear thermo-mechanical analyses. The temperature increase in each rod, $+36\ K$ (graphite) and $+21\ K$ (aluminium), is obviously not an issue as in the case of the MSE septum coils. The Stassi equivalent stresses in the graphite rod are always negligible. For the

aluminium rod, the maximum Von Mises equivalent stress is far below any aluminium alloy tensile yield stress. Furthermore, it has been shown that with material damping ratios of common values, the amplitude of the shock waves is significantly reduced, thus reducing also the peak equivalent stresses.

Acknowledgements

The authors would like to thank E. Chiaveri and L. Bruno for their comments and discussions on the subject, and H. Vincke for providing the original FLUKA input file describing in details the TPSG4 layout in LSS4.

References

[1] B. Goddard, P. Knaus, G. Schröder, W. Weterings, J. Uythoven, *The New SPS Extraction Channel for LHC and CNGS*, CERN-SL-2000-036 BT, July 2000.

[2] A. Fassò, A. Ferrari, P.R. Sala, *Electron - photon transport in FLUKA status*, Proc. of the Monte Carlo 2000 Conference, Lisbon, October 23-26 2000, A. Kling, F. Barão, M. Nakagawa, L. Távora, P. Vaz eds., Springer-Verlag Berlin, p. 59 - 164 (2001).

A. Fassò, A. Ferrari, J. Ranft, P.R. Sala, *FLUKA: Status and Prospective for Hadronic Applications*, Proc. of the Monte Carlo 2000 Conference, Lisbon, October 23-26 2000, A. Kling, F. Barão, M. Nakagawa, L. Távora, P. Vaz eds., Springer-Verlag Berlin, p. 955-960 (2001).

[3] ANSYS, Inc., http://www.ansys.com/, *ANSYS (revision 6.0).*

[4] B. Goddard, P. Knaus, *Beam Loss Damage in a Wire Septum*, CERN-SL-2000-035 BT, July 2000.

[5] G. Ferioli, B. Goddard, P. Knaus, J. Koopman, *Energy Deposition in a Septum Wire*, CERN-SL-2001-029 MD, July 2001.

[6] B. Goddard, E. Carlier, P. Knaus, J. Uythoven, *Equipment Protection Issues for Fast Extraction from SPS to LHC*, Proc. of PAC2001, Chicago, 2001.

[7] J. M. Zazula, M. Ross, S. Péraire, *Thermo-Mechanical Effects Induced by SPS Beam in a Beryllium Rod of the T9 Neutrino Target*, CERN-SL-1995-090 BT/TA and refs. therein, August 1995.

[8] H. Vincke, G. R. Stevenson, D. Forkel-Wirth, *Temperature rise due to the loss of the LHC injected beam in the dummy protection unit installed in ECX4*, CERN TIS-RP/TN/2002-014, March 2002.

[9] SL Materials Database, http://oraweb01:9000/matprop/owa/accisweb.welcome

[10] P. Sievers, *Elastic Stress Waves in Matter Due to Rapid Heating by an Intense High-Energy Particle Beam*, CERN LAB.II/BT/74-2, June 1974.

Known Parameters	*Values*	*Units*
Diluter Physical		
Max width	16.0	mm
Max length	3250 (C: 2350, Al: 900)	mm
Min height	20	mm
Drift to septum	120	mm
Max septum Temp	100	ºC
Beam		
Momentum	450	GeV/c
Time structure	25 ns bunches x 72 x 4	
Intensity	$1.1x10^{11}$ ($1.7x10^{11}$) $3.2x10^{13}$ ($4.9x10^{13}$)	Protons per bunch Total protons
Beam size at TPSG	0.95 / 0.4	σ_H / σ_V in mm
Kickers		
Rise time	1.1	μs
Kick strength	41	Opening in mm
Bunches on TPSG4	21	

Table 1: Summary of the beam characteristics, diluter dimensions and other parameters assumed for the analysis (the numbers in parenthesis for the beam intensity refer to the ultimate LHC beam parameters)

	Graphite	**Aluminium**	**Copper**
Density ($Kg.m^{-3}$)	1850	2700	8960
Specific Heat ($J.Kg^{-1}.K^{-1}$)	510	890	388
Thermal Conductivity ($W.m^{-1}.K^{-1}$)	93	125	400
Thermal Expansion Coefficient ($.10^{-6}$)	2.97	23.58	17.6
Elastic Modulus (MPa)	9960	71680	115000
Poisson's Ratio	0.15	0.34	0.41
K (compressive / tensile yield stress)	3.3	1	1
Interaction length (cm)	48.76	39.41	15.06
Melting point (ºC)	3650	660	1083
Max design temperature (ºC)	1000	200	100

Table 2: Graphite, aluminium and copper material properties

Specific heat evolution with temperature, T (K):

Graphite: $c_p(T) = 528.75 - 205.9\,T^{1/3} + 154.21\,T^{1/2} - 1.53\,T + 9.15x10^{-5}\,T^2$

Aluminium: $c_p(T) = 890.54 + 1.53\,T$

Copper: $c_p(T) = 381.12 + 0.16\,T - 1.09x10^{-4}\,T^2$

Temperature (°C)	Time	X=0		X=max(J/m^3)		X=l/2		X=l	
		C	Al	C	Al	C	Al	C	Al
	End of pulse	561	196	822	270	583	144	233	56
	1 s	37	135	85	160	259	97	166	71

Peak Stresses	C				Al		
	Stress	Time	Location	Value (MPa)	Time	Location	Value (MPa)
	S1	0.06	Max	-36.5	0.015 ms	Max	-512
	S2	0.03 ms	Max	-43	0.015 ms	Max	-752
	S3	0.46 ms	Max	-64	0.015 ms	Max	-881
	Von Mises	0.015 ms	L/2	48	0.021 ms	Max	**684**
	Stassi	0.015 ms	L	**16**			

	C Maximum Oscillation		Al	
	Transversal 27 µs	Longitudinal 2 ms	Transversal 11 µs	Longitudinal 0.4 ms
S1	± 25 MPa / X=l/2	± 13 MPa / X=l/2	± 320 MPa / X=Max	± 260 MPa / X=0
S2	± 6 MPa / X=l/2	± 7 MPa / X=Max	± 170 MPa / X=0	± 150 MPa / X=Max
S3	± 4 MPa / X=l/2	± 7 MPa / X=Max	± 170 MPa / X=0	± 200 MPa / X=0

Table 3: Summary of maximum temperatures and stresses on beam axis for both graphite and aluminium rods. "Worst case" (without material damping, 3-D model)

Temperature (°C)	Time	X=0		X=max(J)		X=l	
		C	Al	C	Al	C	Al
	End of sweep	26	36	56	41	43	22
	10000 s	44	37	42	37	37	36

Peak Stresses	C				Al		
	Stress	Time	Location	Value (MPa)	Time	Location	Value (MPa)
	S1	End sweep	Max	-14.2	3.5 µs	Max	-224
	S2	End sweep	Max	-14.2	3.5 µs	Max	-224
	S3	4.8 ms	X=l	-14.5	26.5 µs	Max	-226
	Von Mises	4 µs	X=l	1	0.4 ms	X=l	**43**
	Stassi			**~0**			

	Maximum Oscillation		Maximum Oscillation	
	Longitudinal 1.8 ms	Transversal 10 µs	Longitudinal 0.25 ms	Transversal 2.2 µs
S1	± 0.38 MPa / X=l	± 0.2 MPa / X=Max(J)	± 23 MPa / X=Max(J)	± 19 MPa / X=Max(J)
S2	± 0.12 MPa / X=Max(J)	± 0.08 MPa / X=Max(J)	± 17 MPa / X=0	± 10 MPa / X=Max(J)
S3	± 0.45 MPa / X=0	± 0.5 MPa / X=0	± 25 MPa / X=l	± 10 MPa / X=Max(J)

Table 4: Summary of maximum temperatures and stresses for both graphite and aluminium rods. "Sweep case" (without material damping, 2-D model)

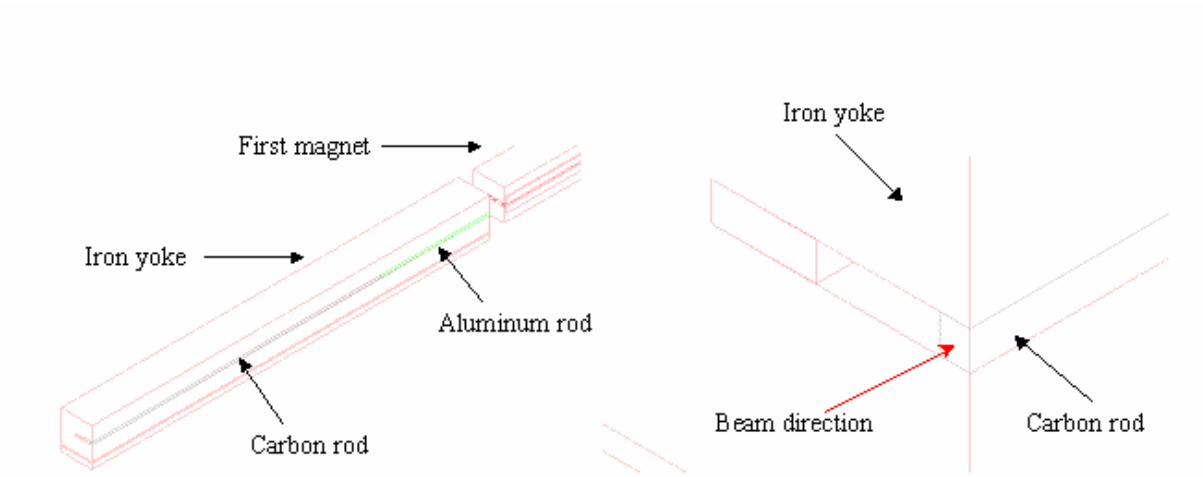

Figure 1: The TPSG4 diluter used to protect the extraction magnets in ECX4 (taken from Ref. [8])

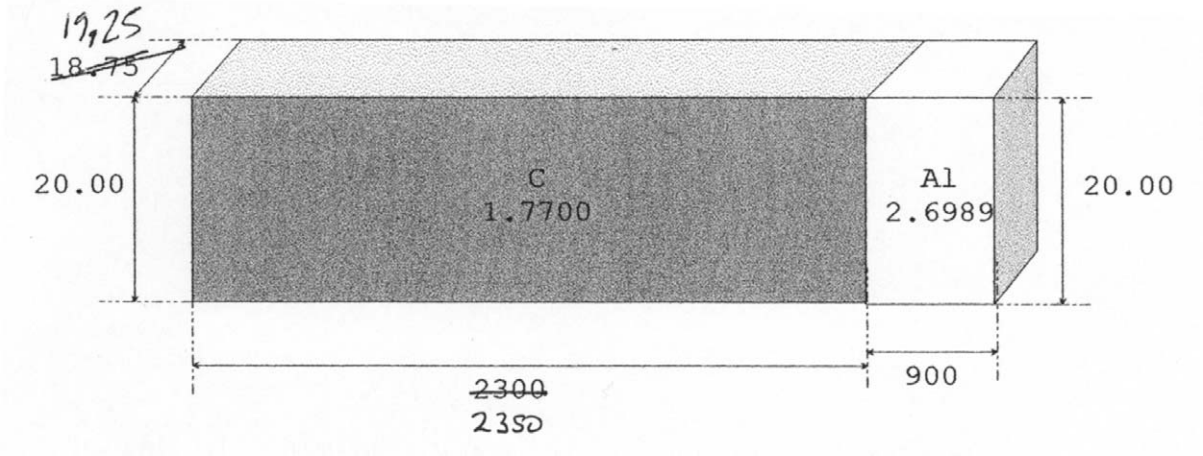

Figure 2: The total length of the diluter is 325 cm and its cross-section is 1.925 x 2.0 cm^2. The first 235 cm consists of carbon followed by 90 cm of aluminium

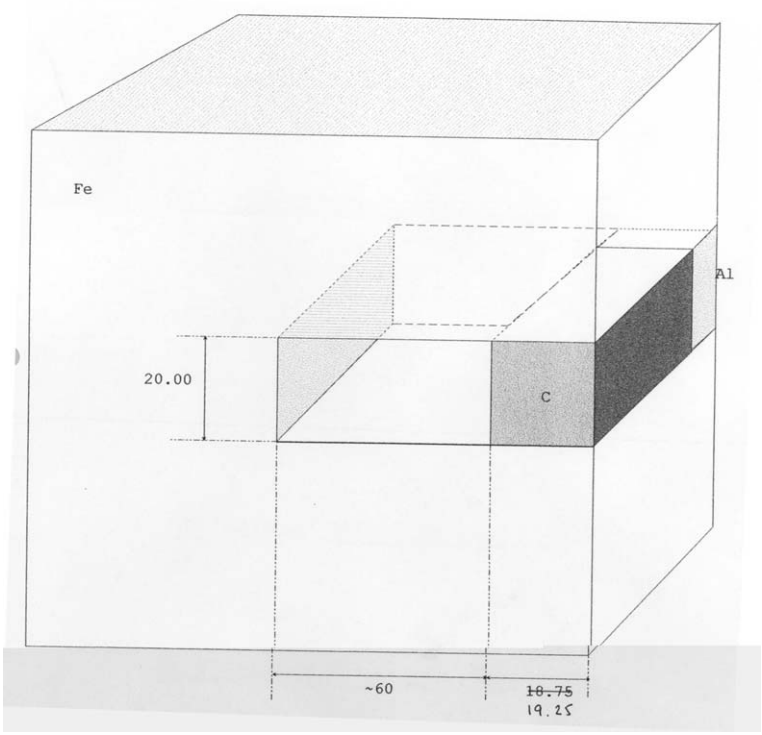

Figure 3: Diluter structure surrounded by an iron yoke (outer dimensions: 25.6 x 25.2 cm^2)

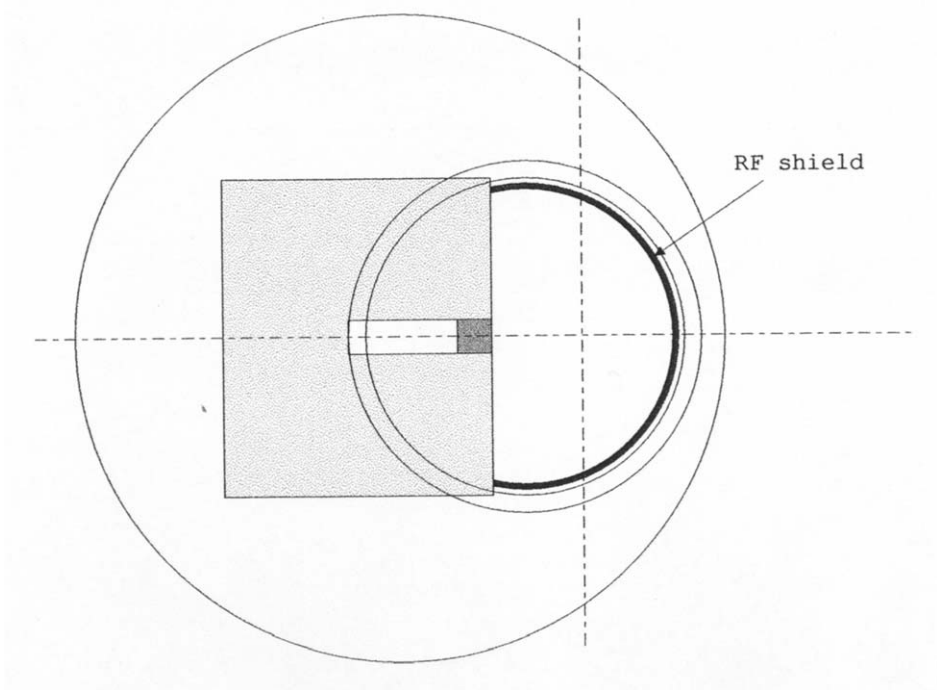

Figure 4: RF shield

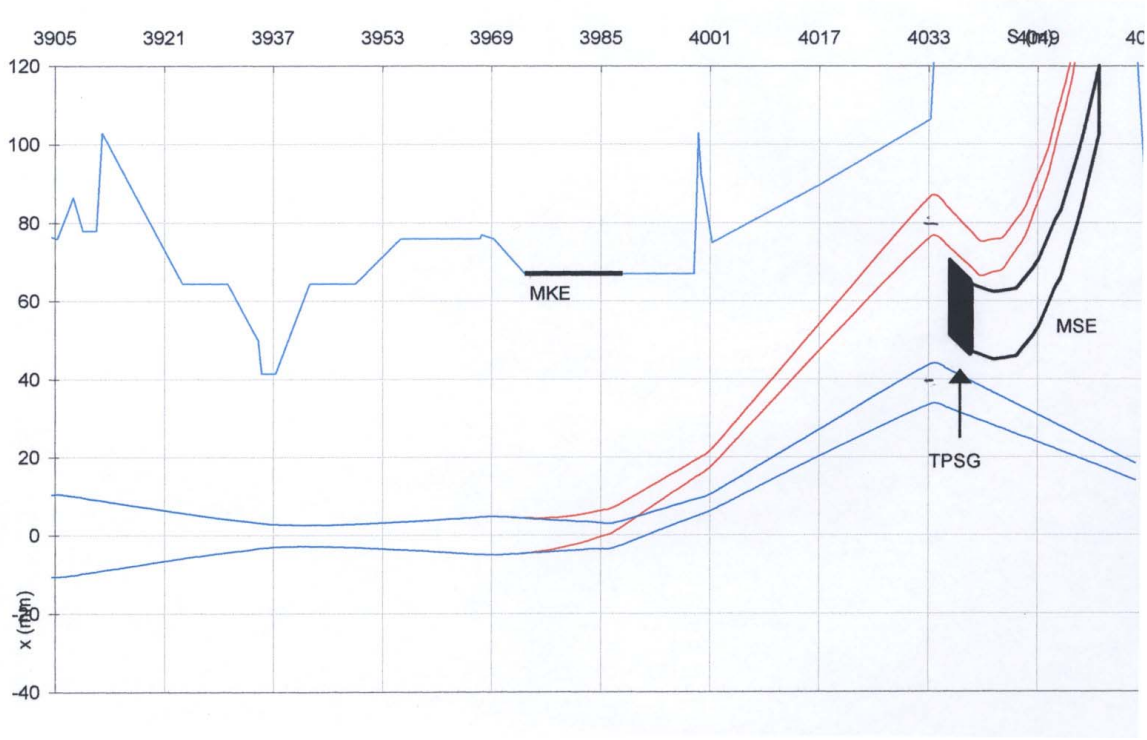

Figure 5: Trajectories of the LHC beam in the LSS4 extraction channel

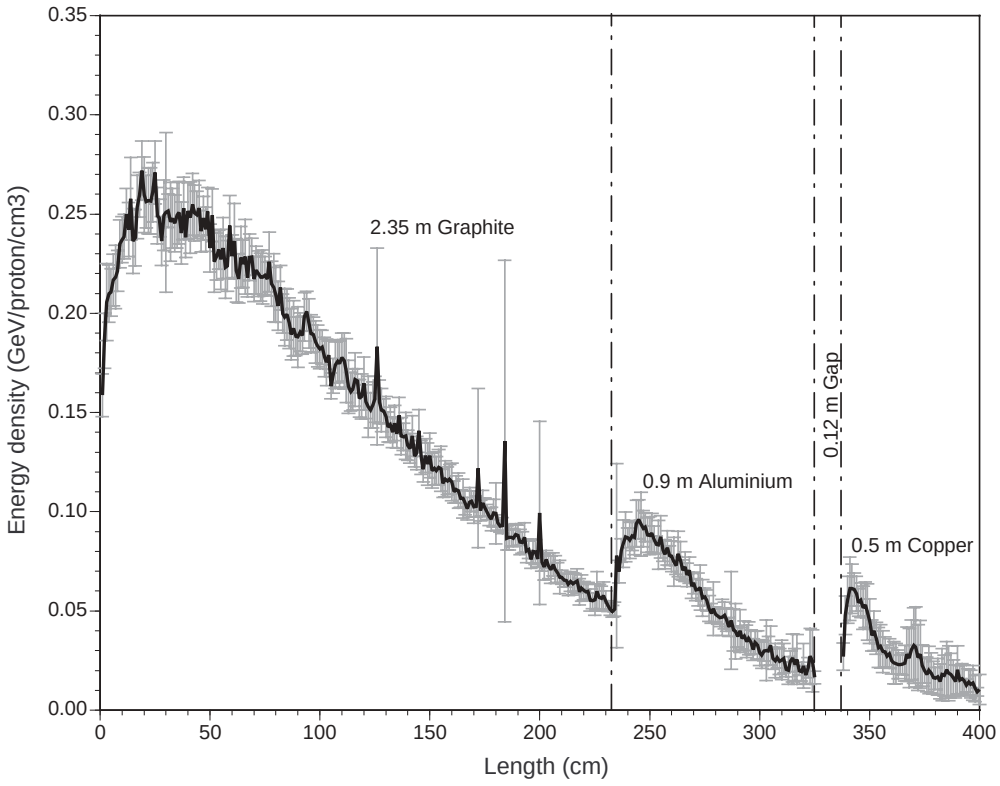

Figure 6: Calculated energy density distribution in diluter and MSE coil (*4.9x10^{13}* protons, *450 GeV/c*)

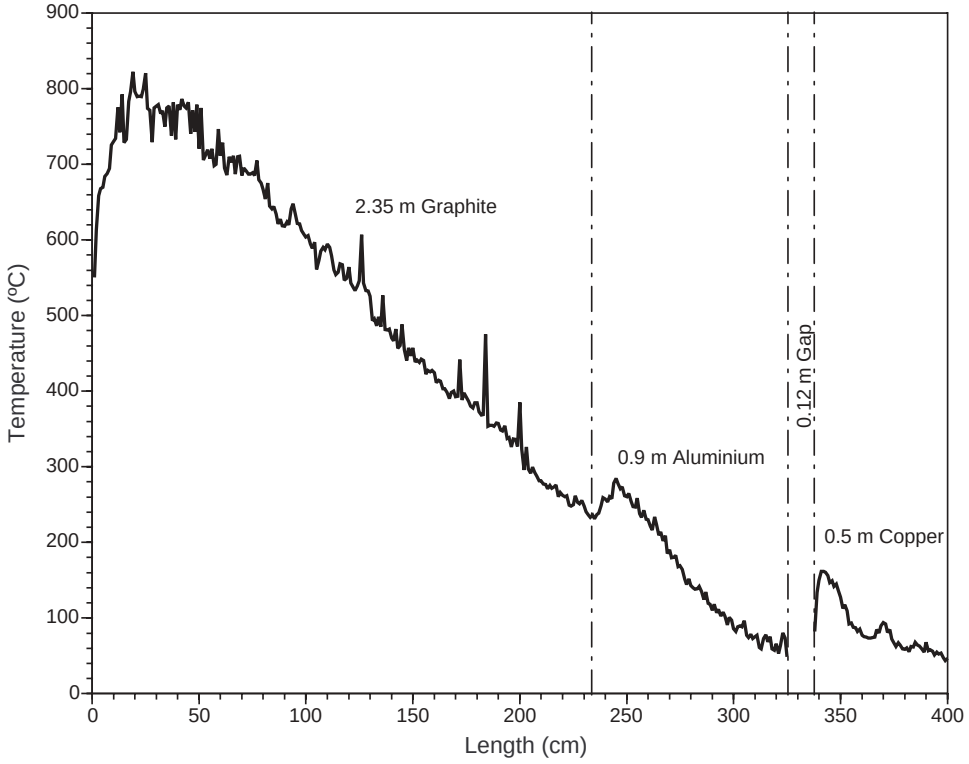

Figure 7: Calculated temperature profile in diluter and MSE coil (*4.9x10*^{13} protons, *450 GeV/c*)

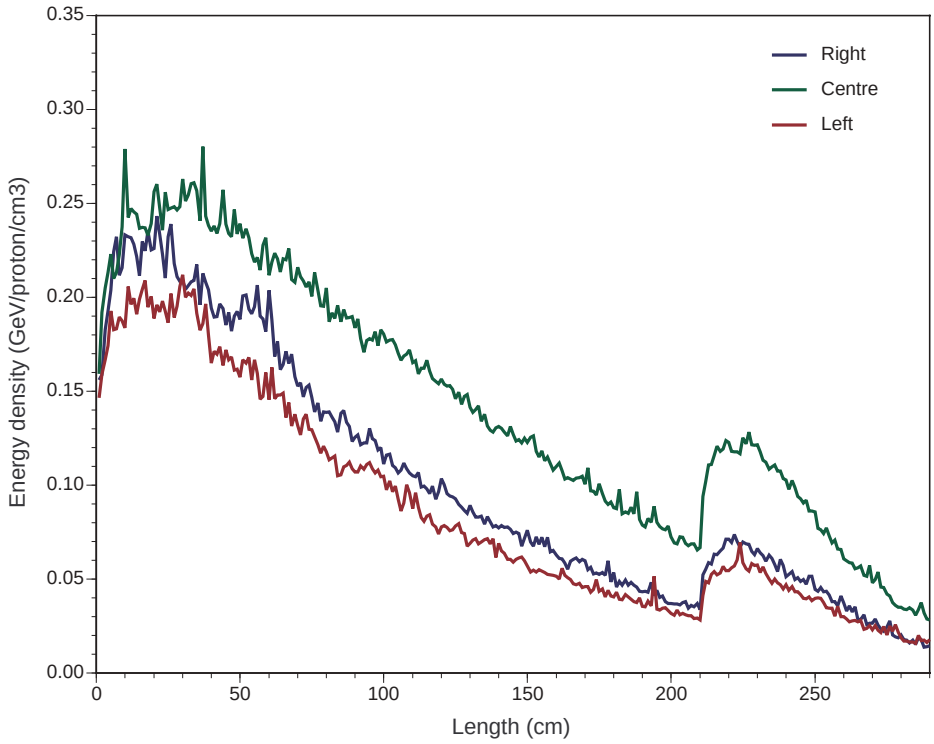

Figure 8: Calculated energy density distribution in the TPSG4 diluter (*1.1x10*^{11} protons, *450 GeV/c*)

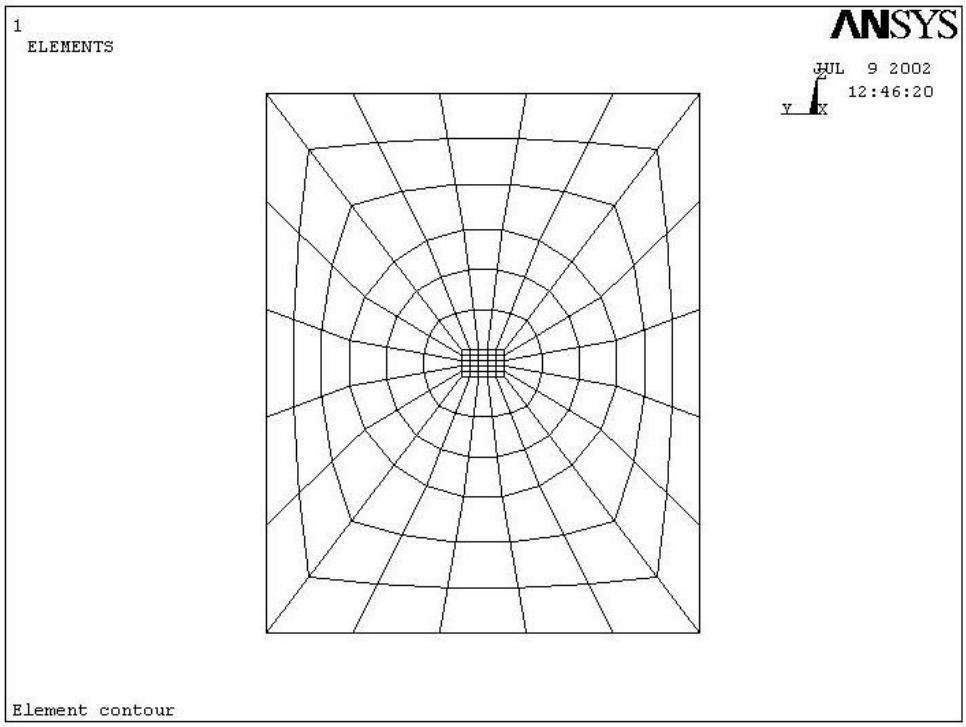

Figure 9: Element contours in a cross-section (3-D model, worst case)

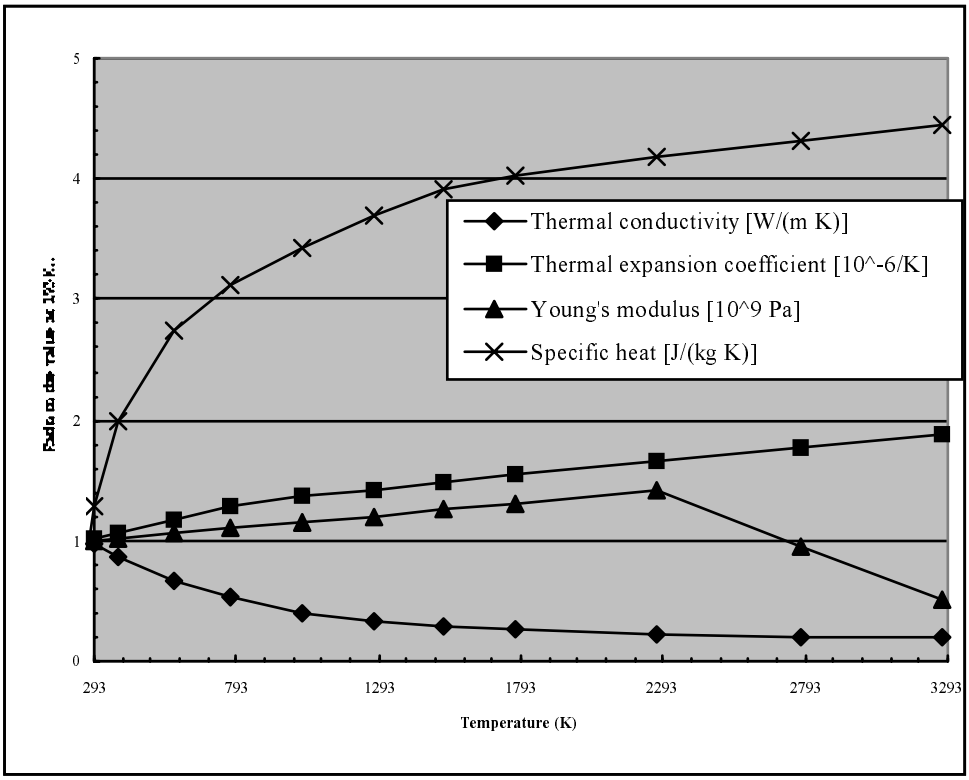

a: Graphite

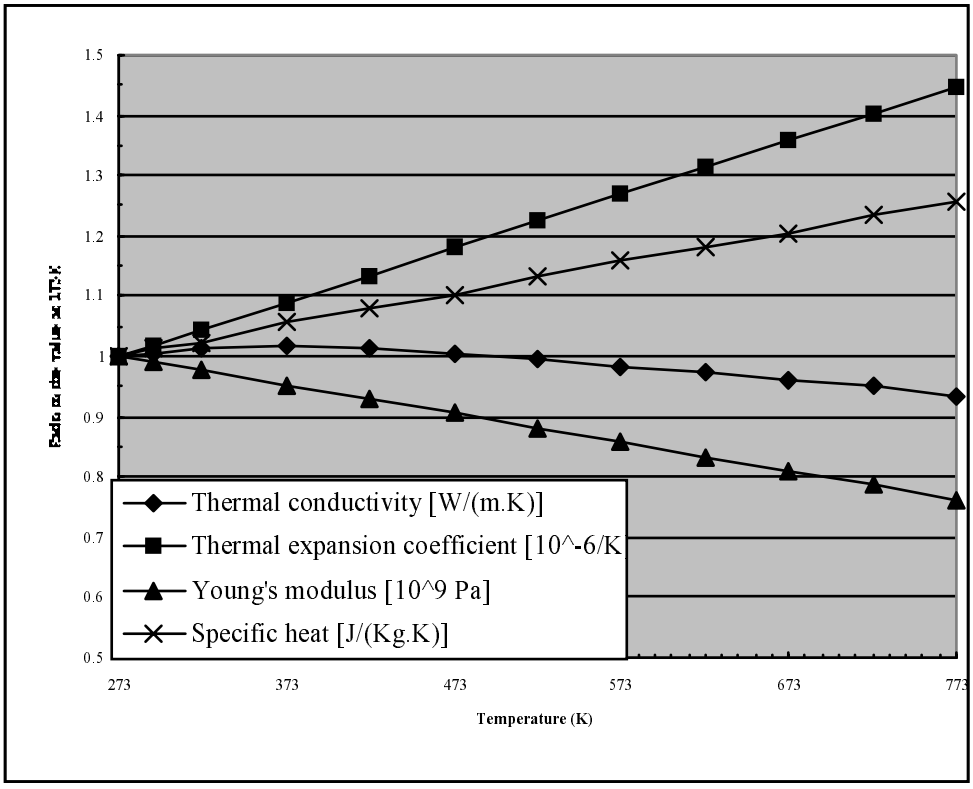

b: Aluminium

Figure 10: Material temperature-dependent properties

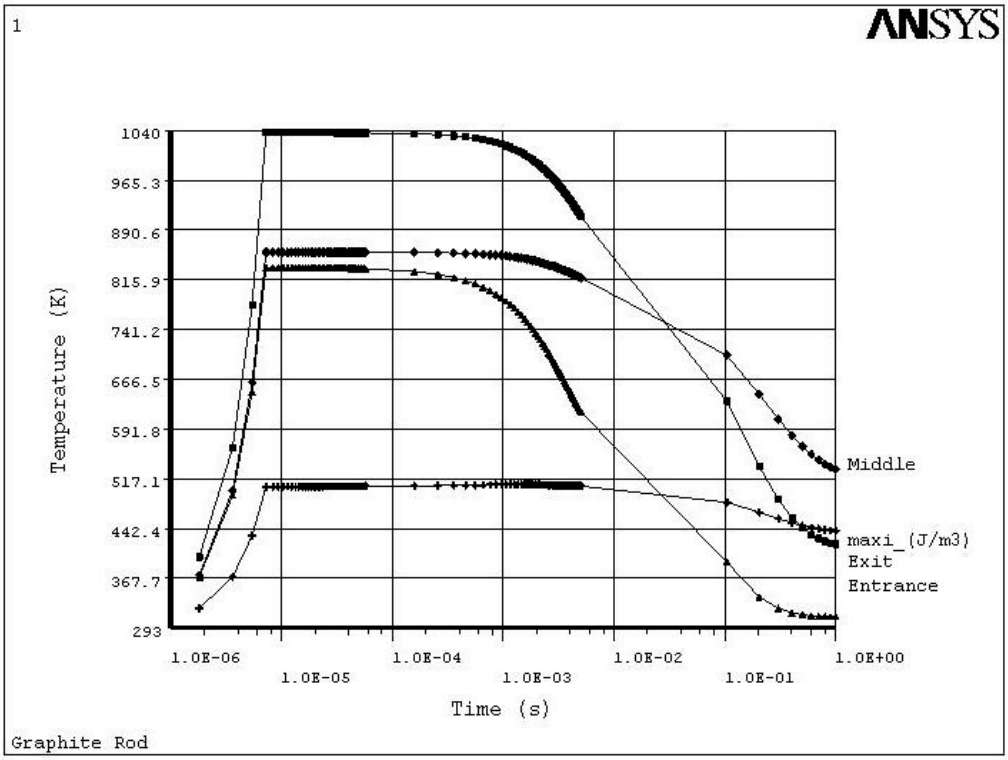

a: Graphite rod

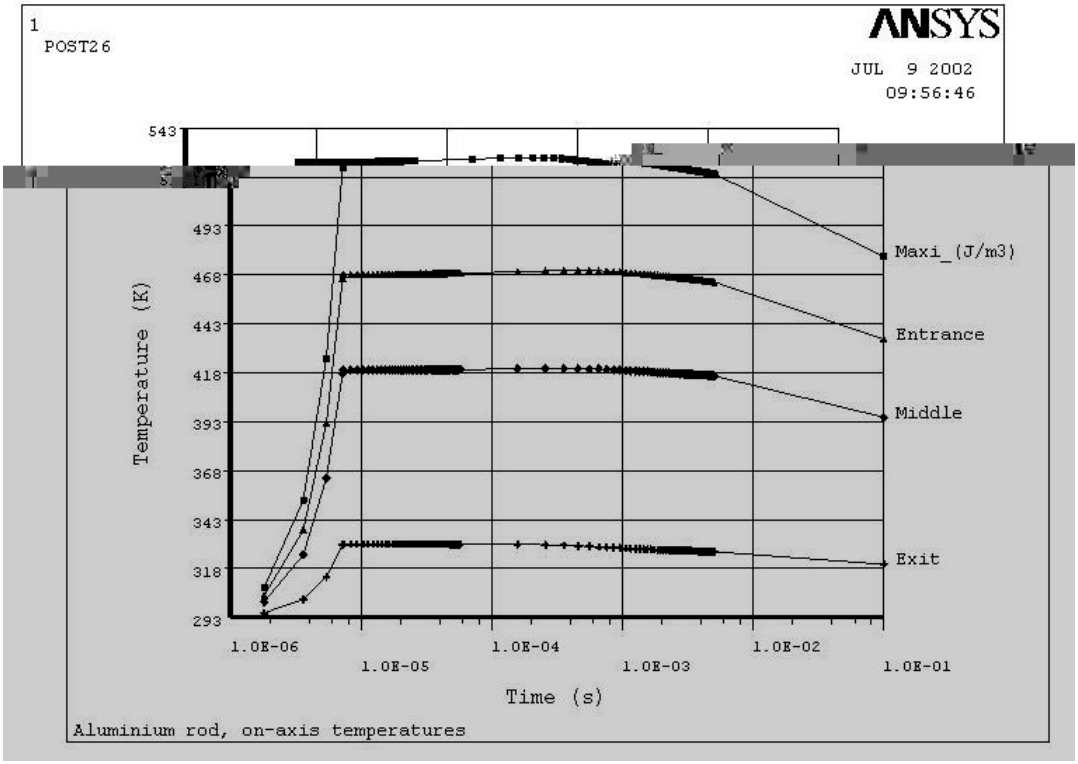

b: Aluminium rod

Figure 11: Time evolution of the on-axis temperatures in four cross-sections

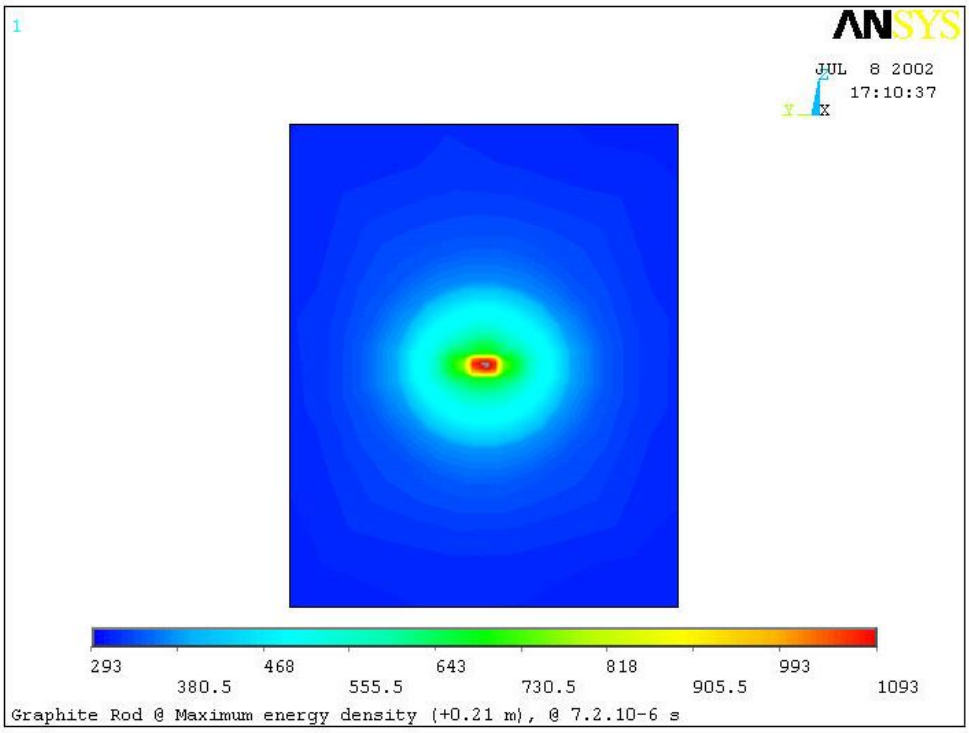

a: Graphite rod

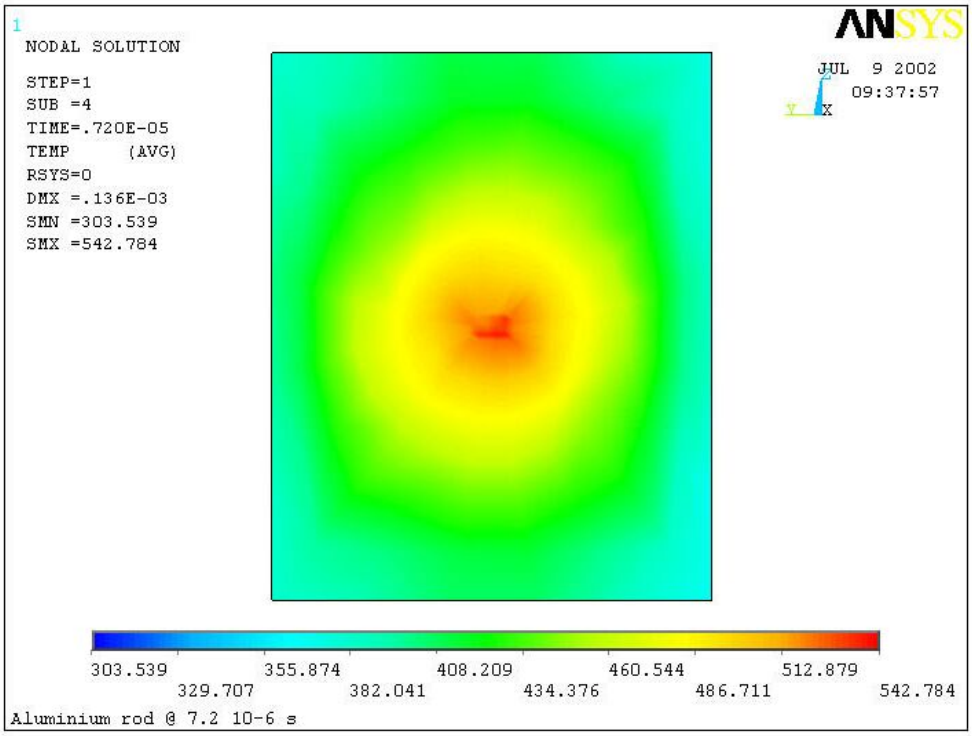

b: Aluminium rod

Figure 12: Temperature distribution in the maximum energy density cross-section, at the end of the pulse

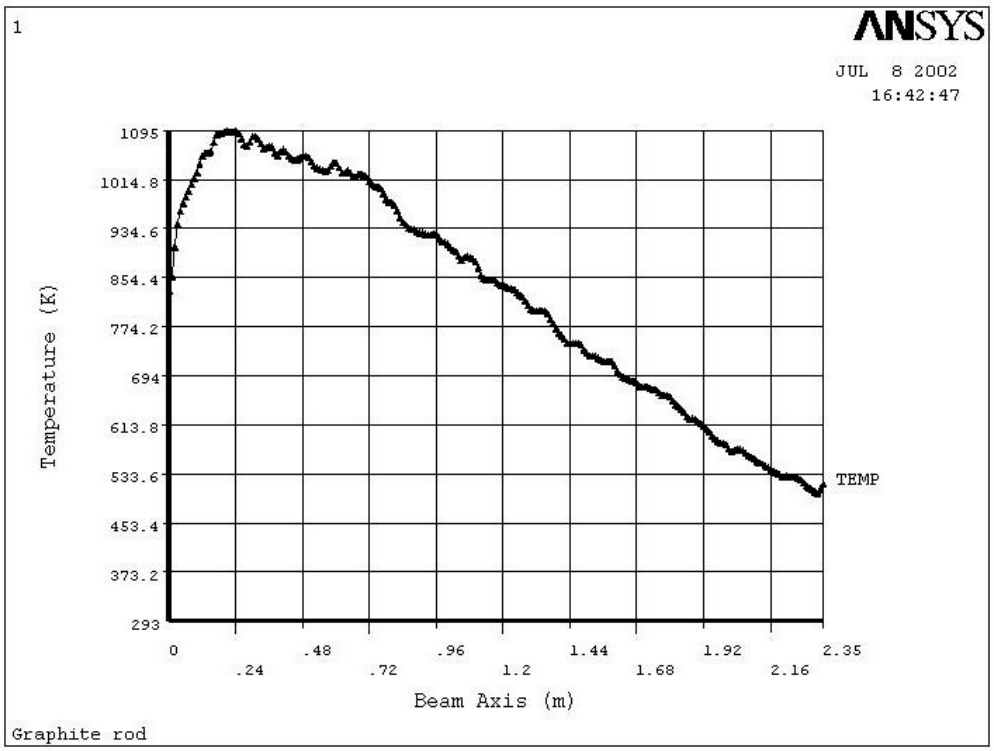

a: Graphite rod

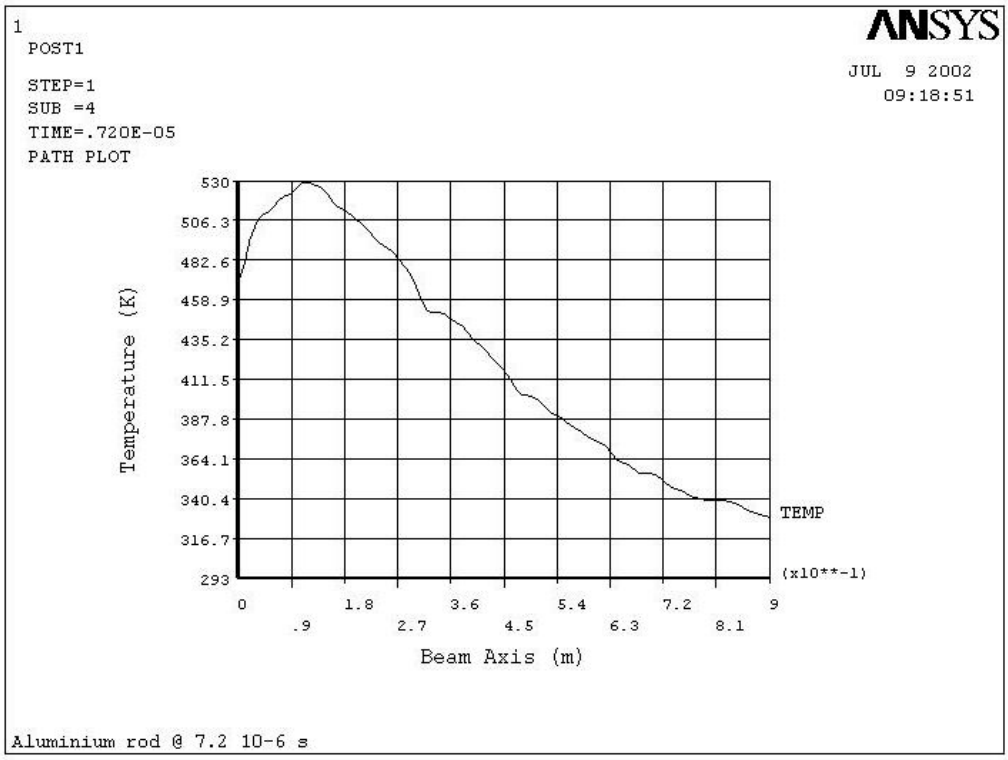

b: Aluminium rod

Figure 13: On-axis temperature distribution, at the end of the pulse

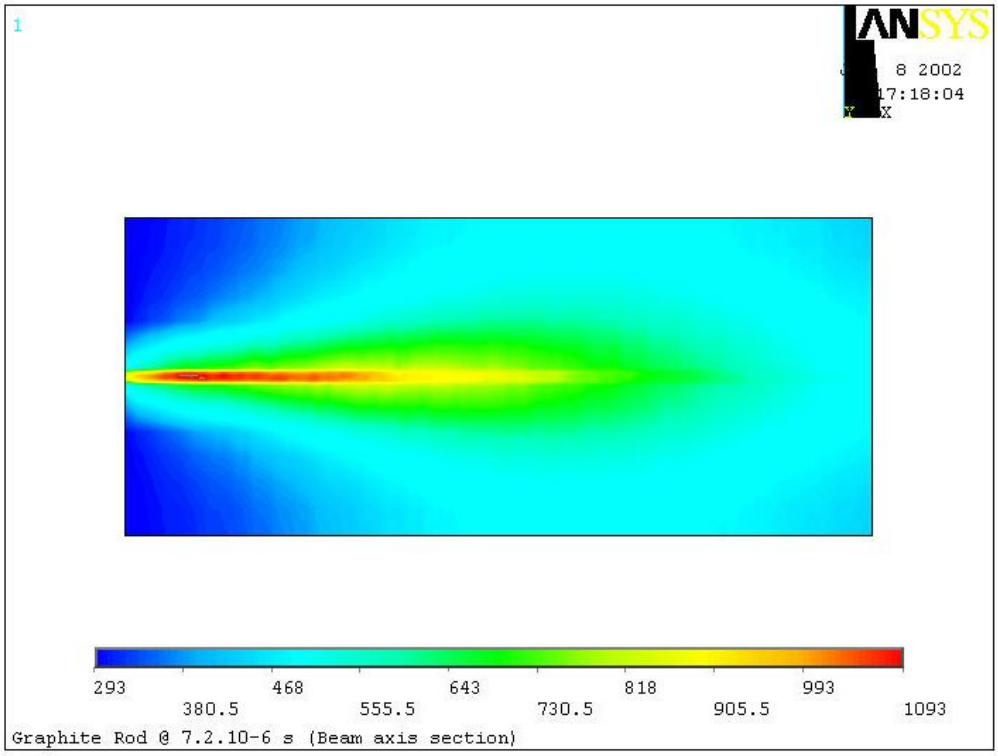

a: Graphite rod (the vertical axis has been magnified by 50)

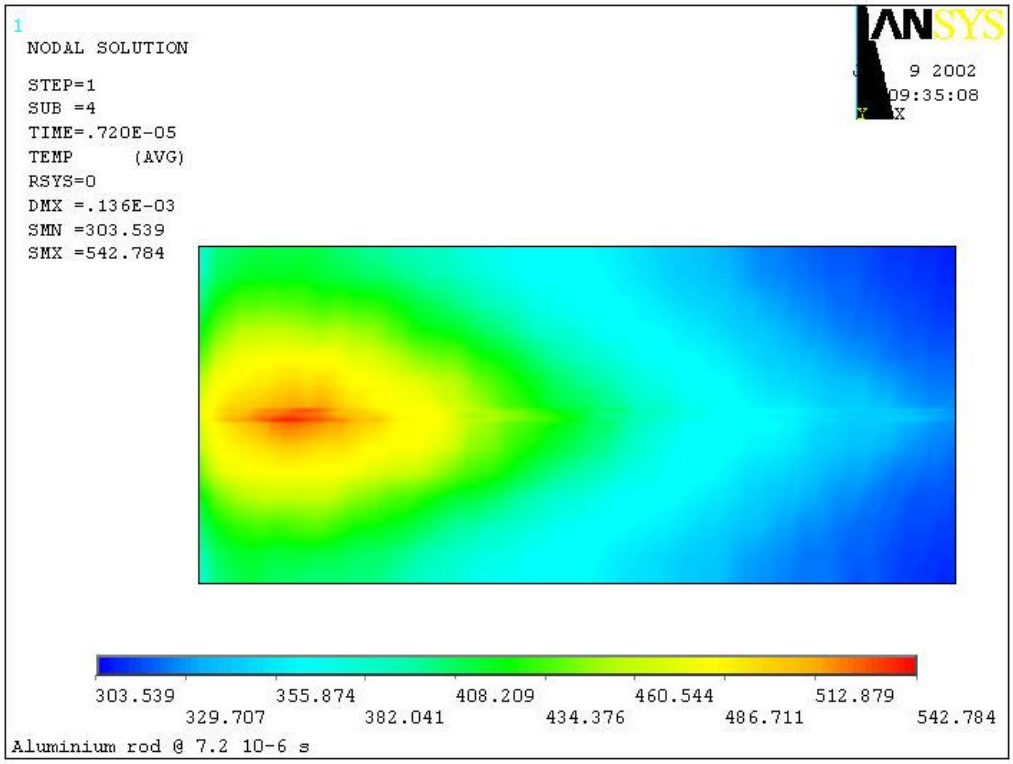

b: Aluminium rod (the vertical axis has been magnified by 20)

Figure 14: Temperature distribution in a longitudinal section, at the end of the pulse

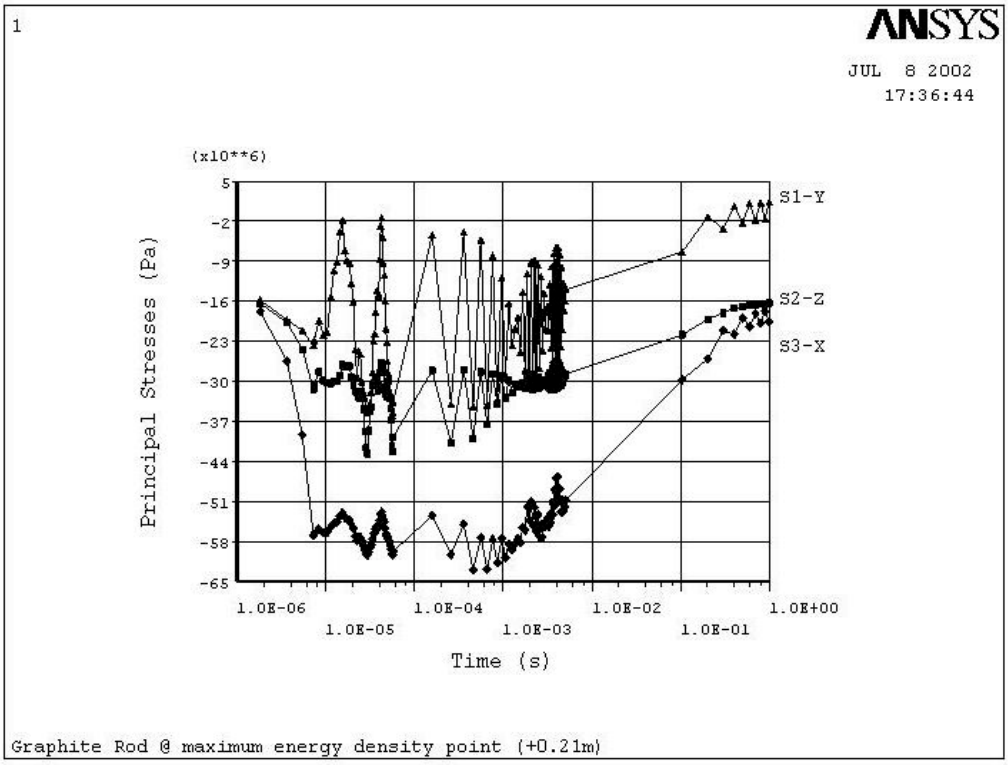

a: Graphite rod

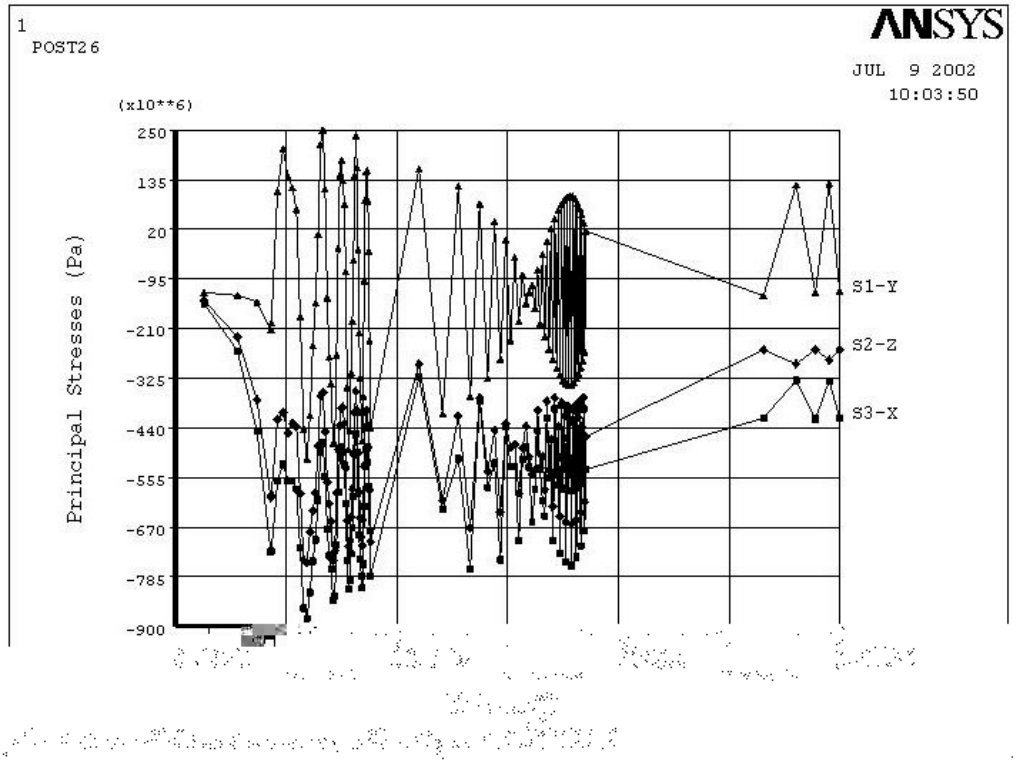

b: Aluminium rod

Figure 15: Time evolution of the principal stresses at point of maximum energy density

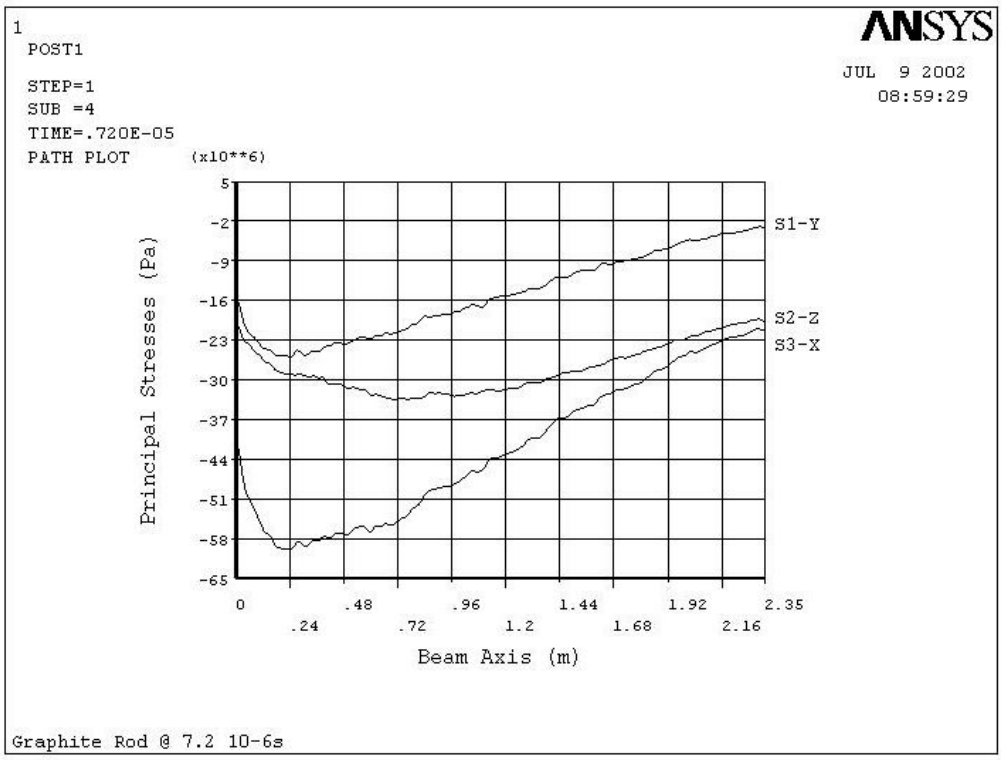

a: Graphite rod

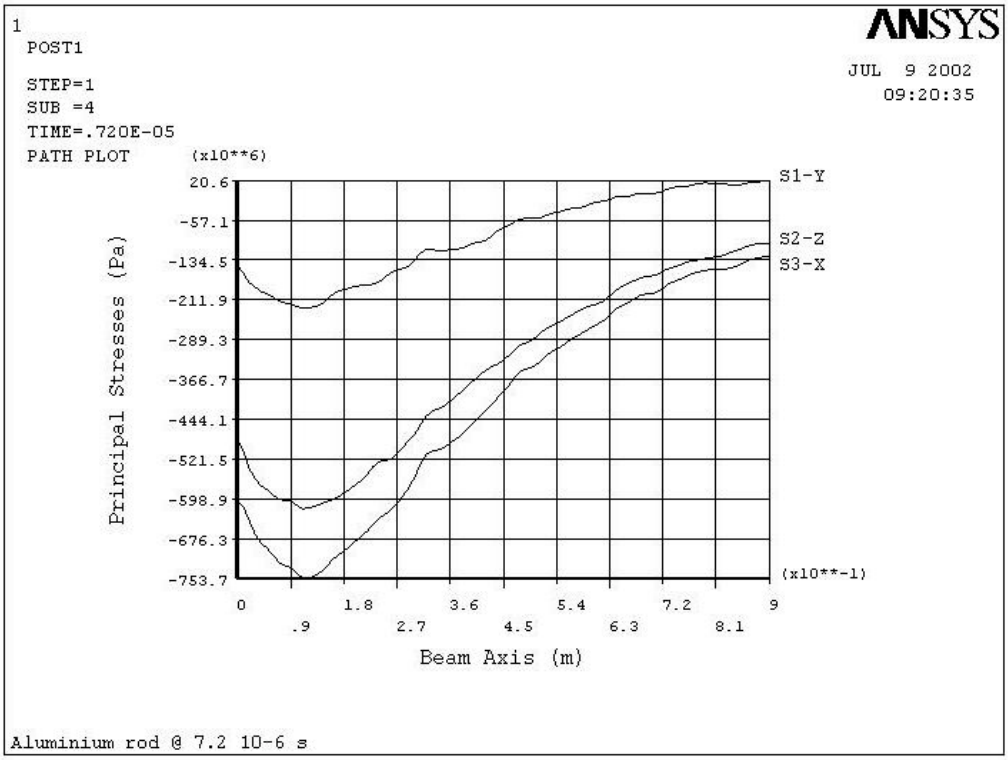

b: Aluminium rod

Figure 16: Principal stresses along beam axis, at the end of the pulse

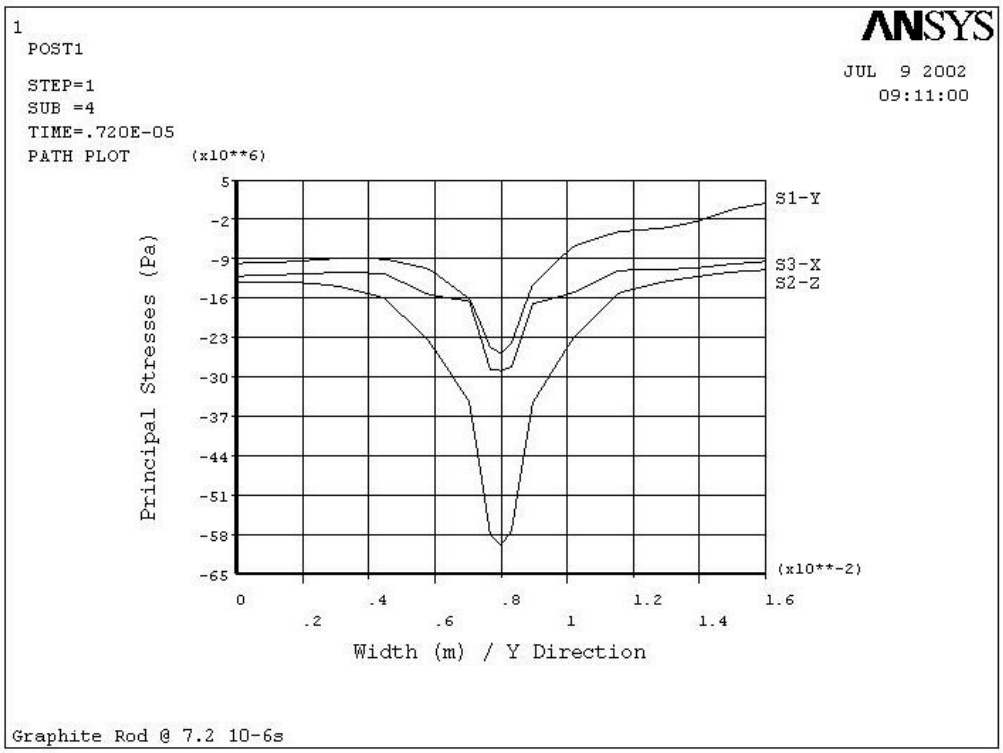

a: Graphite rod

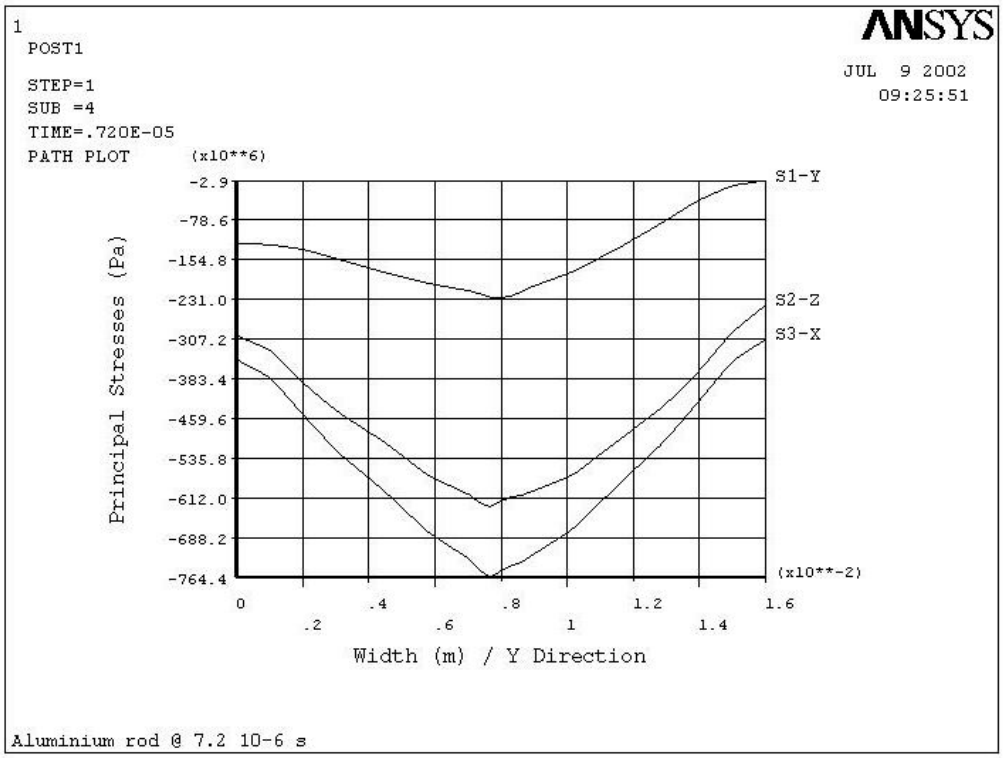

b: Aluminium rod

Figure 17: Distribution of the principal stresses in the maximum energy density section, at the end of the pulse

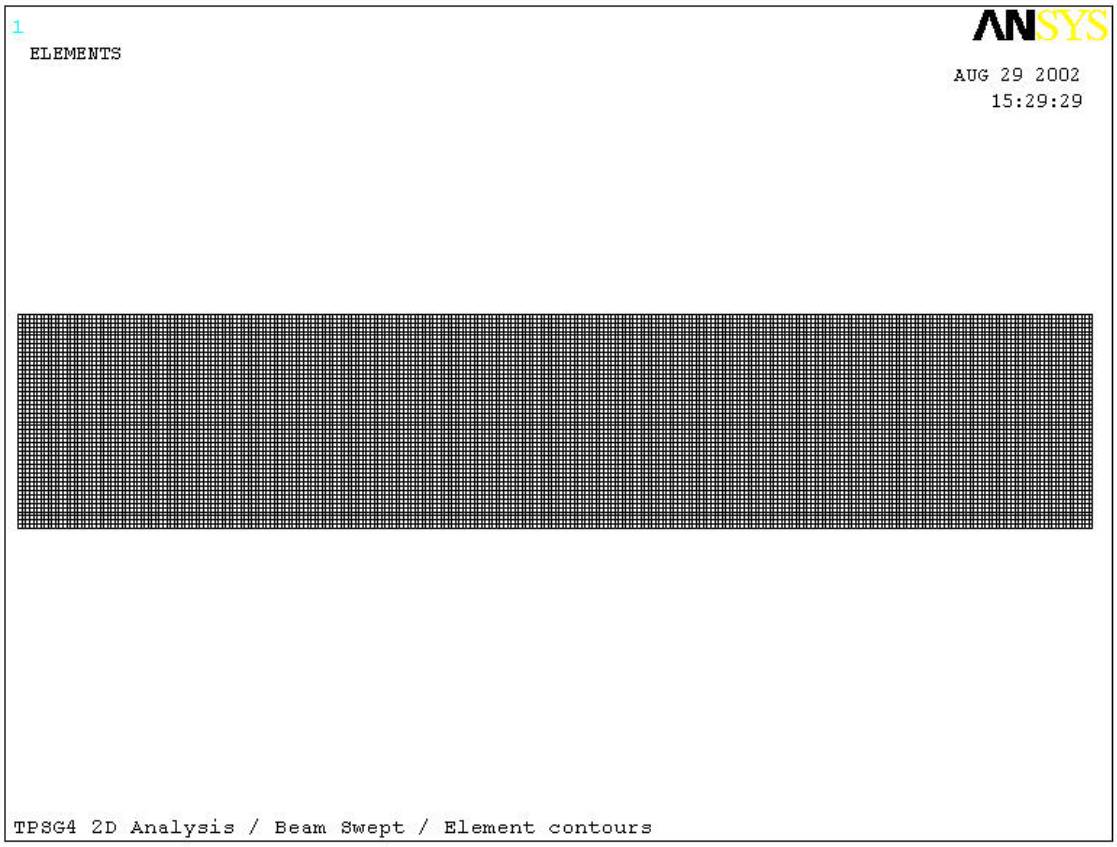

Figure 18: 2D Element contour (sweep case)

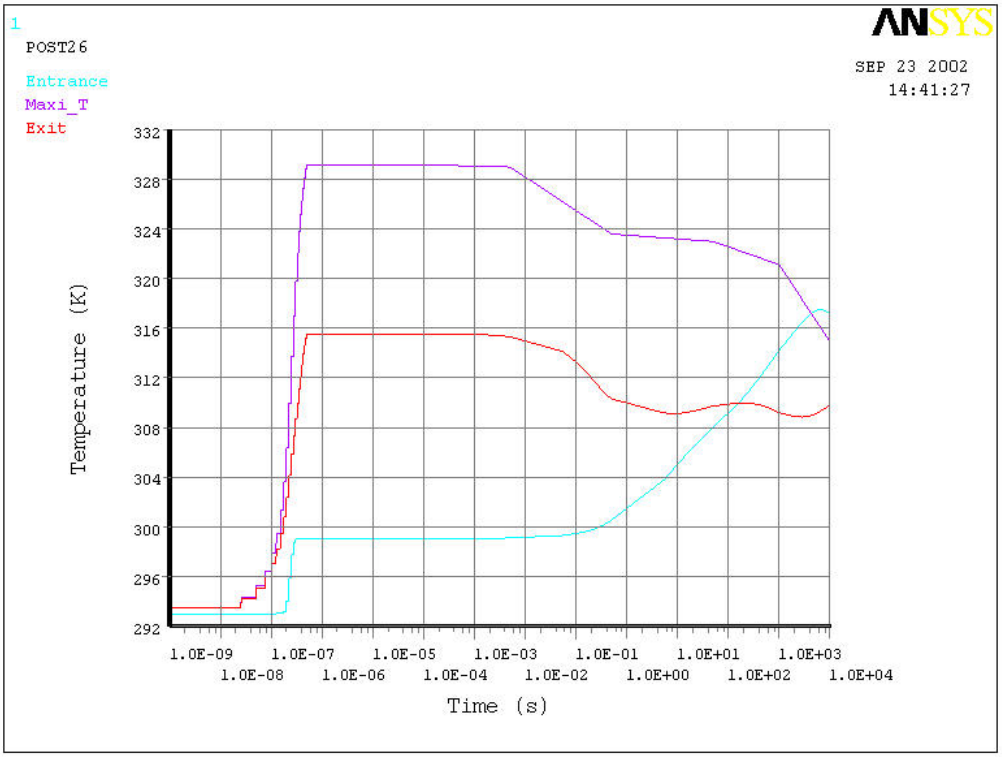

A: Graphite

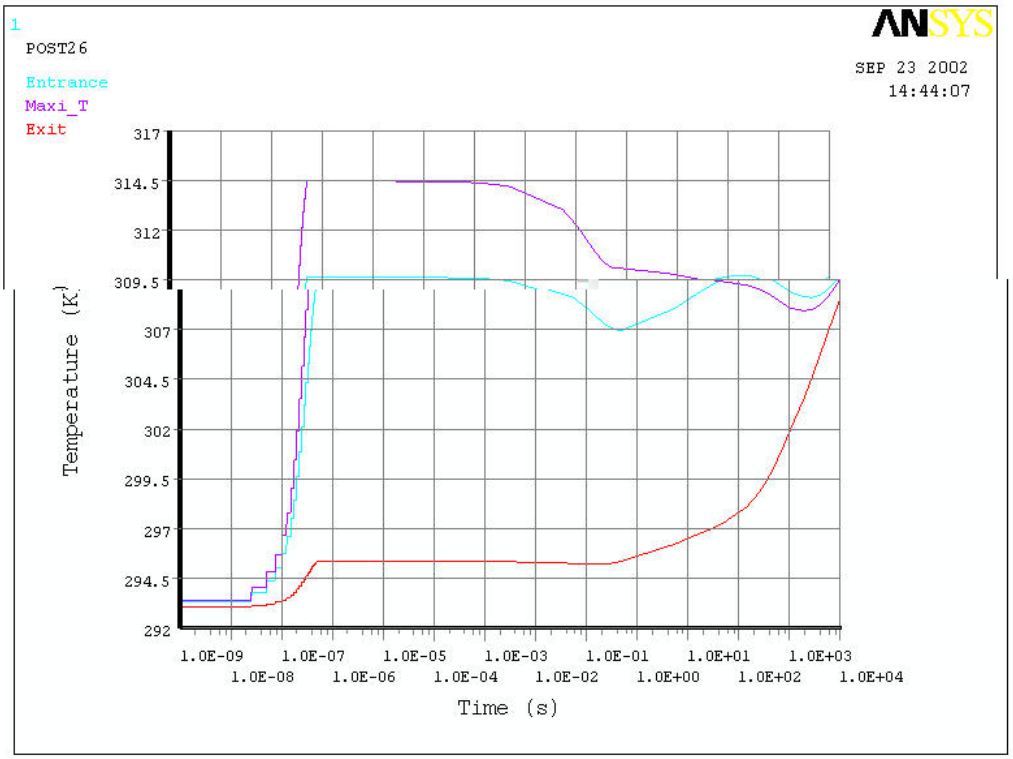

B: Aluminium

Figure 19: Time evolution of the on-axis temperatures

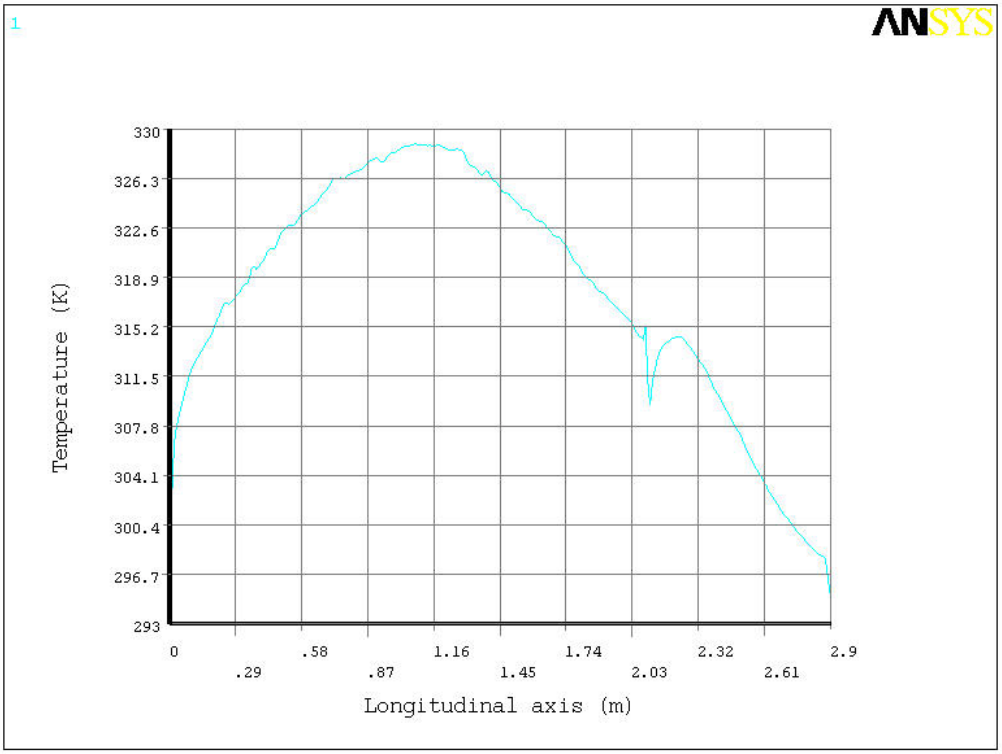

A: on-axis temperatures

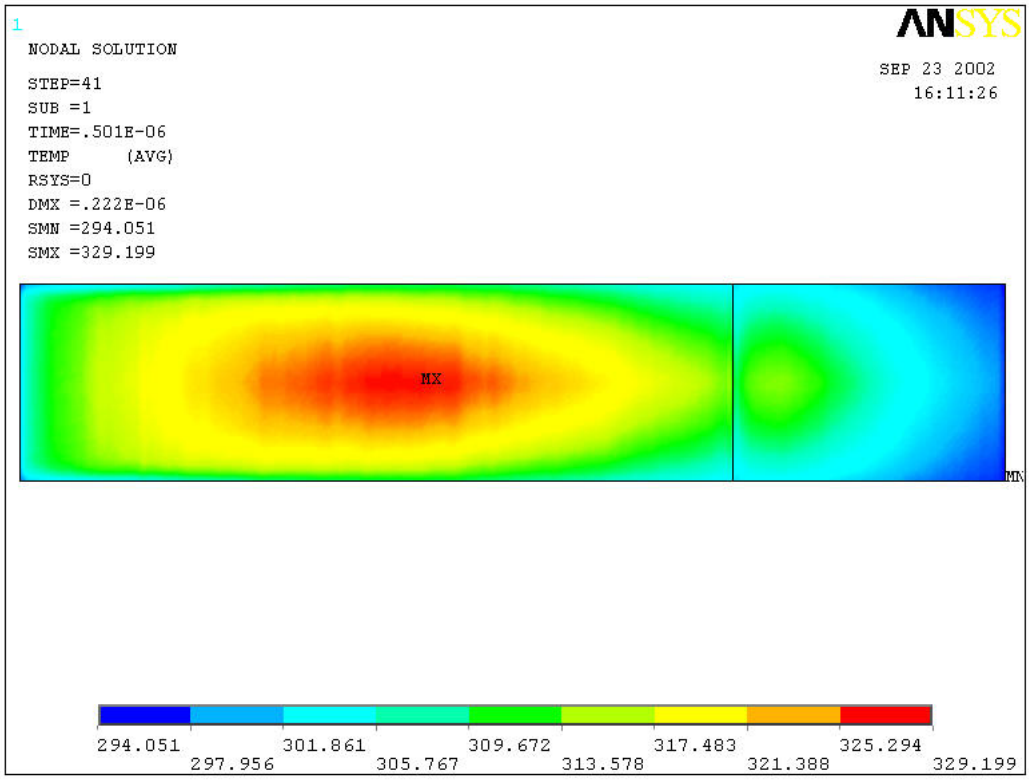

B: 2D distribution (Y axis magnified by 30)

Figure 20: Temperature distributions at the end of the sweep

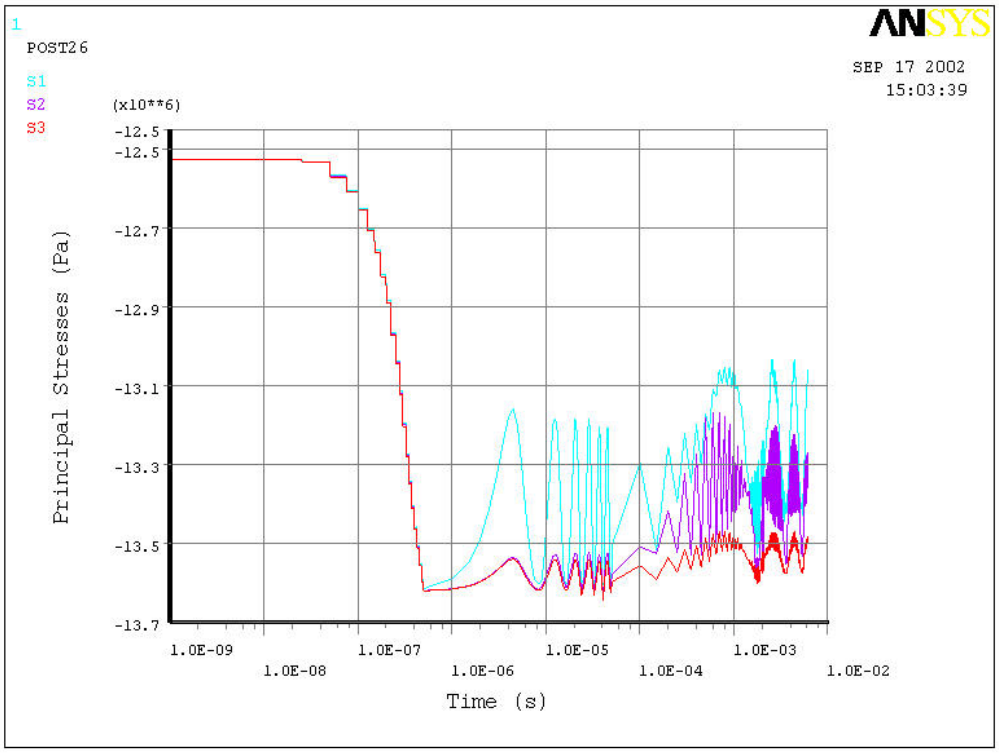

A: Graphite rod

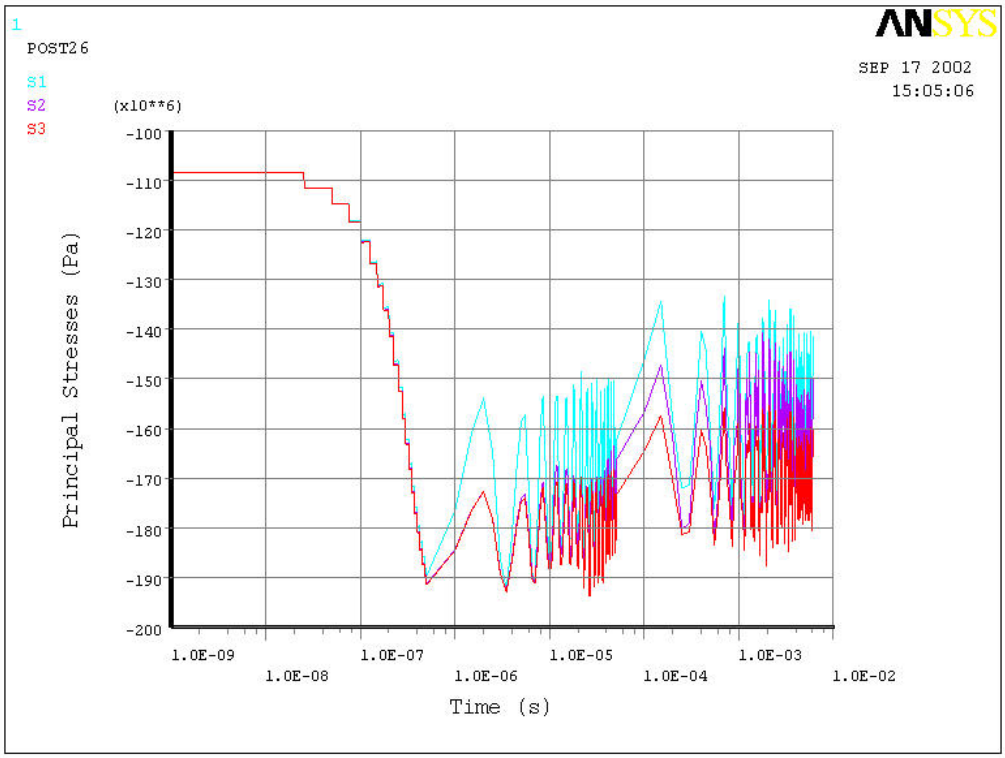

B: Aluminium rod

Figure 21: Time evolution of the principal stresses at point of maximum thermal load.

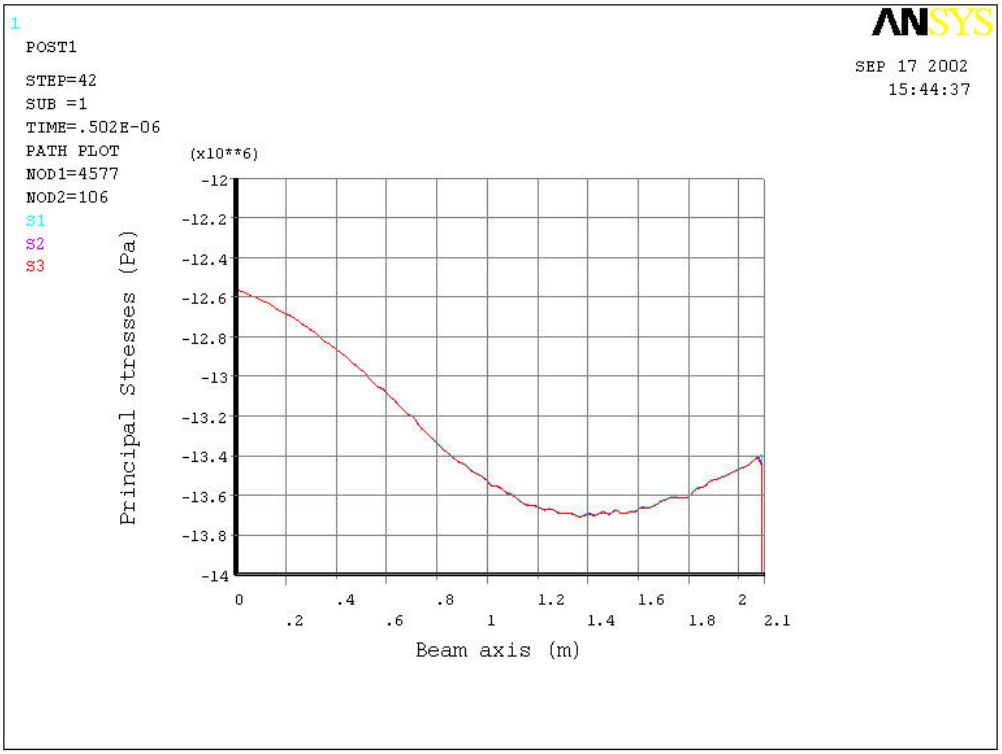

A: Graphite rod

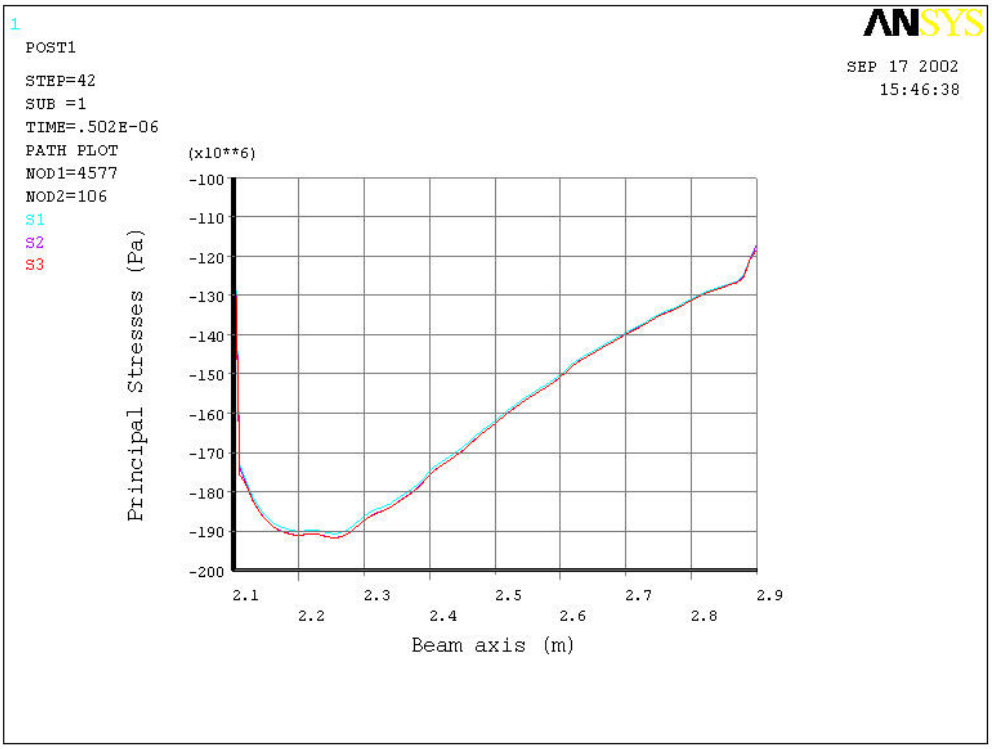

B: Aluminium rod

Figure 22: Principal stresses along beam axis, at the end of the sweep.

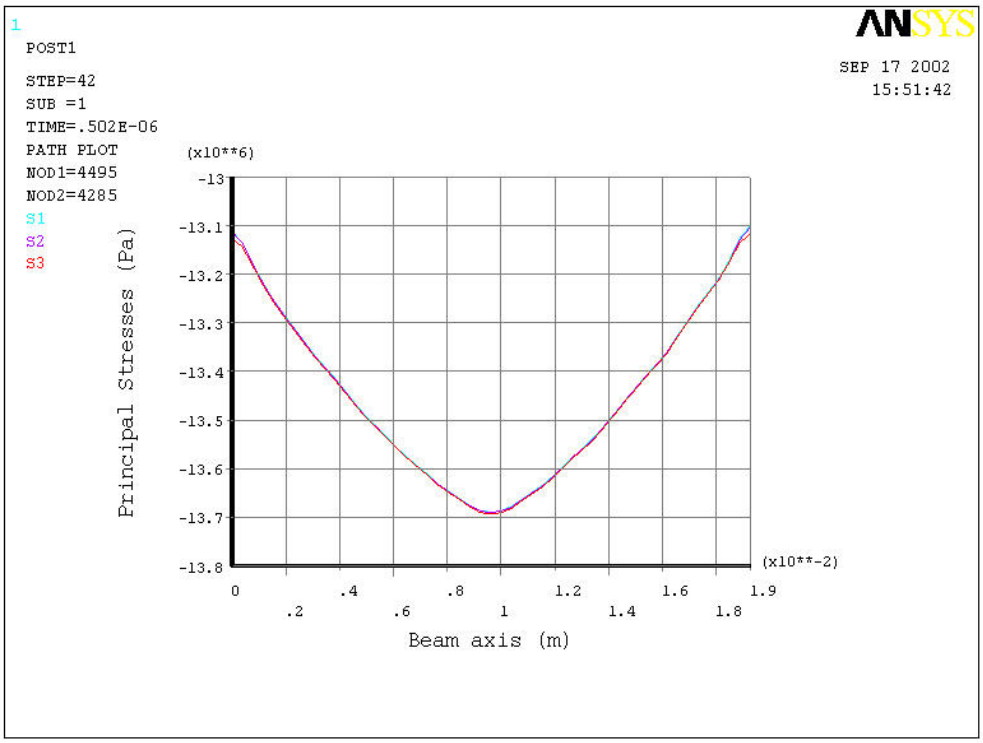

A: Graphite rod

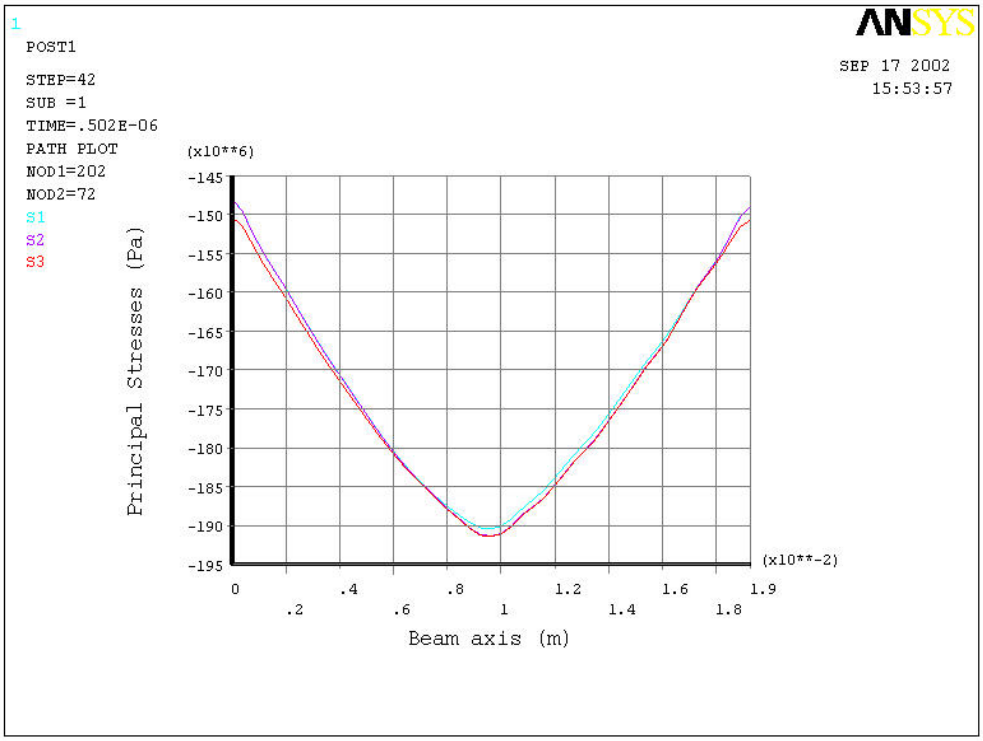

B: Aluminium rod

Figure 23: Distribution of the principal stresses in the maximum thermal load section, at the end of the sweep.

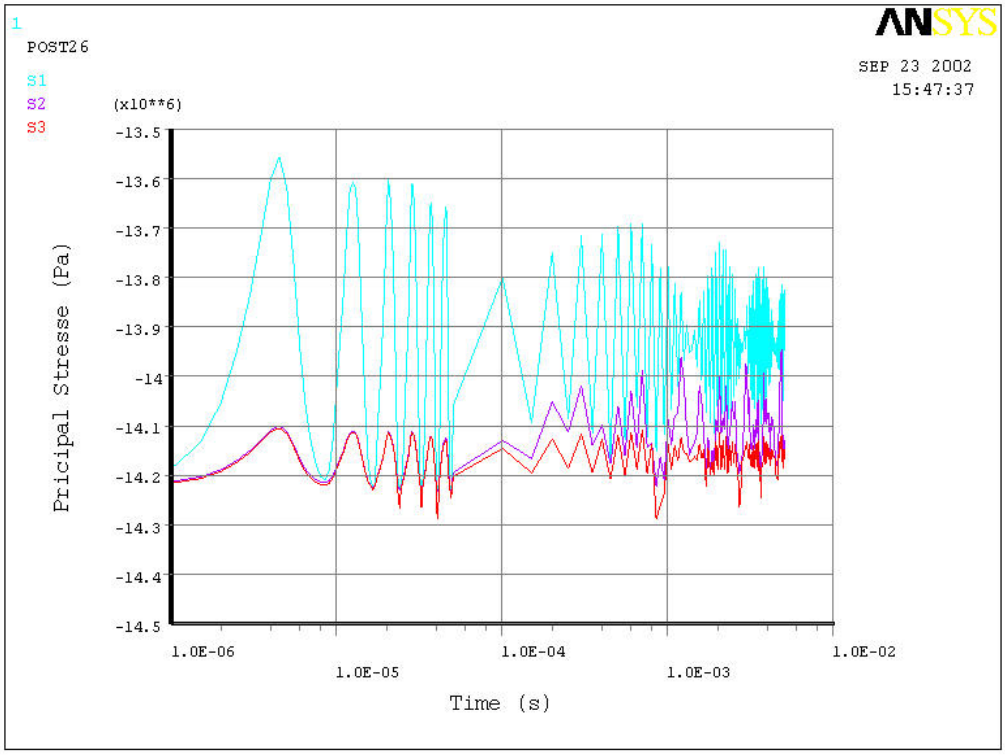

A: Without damping

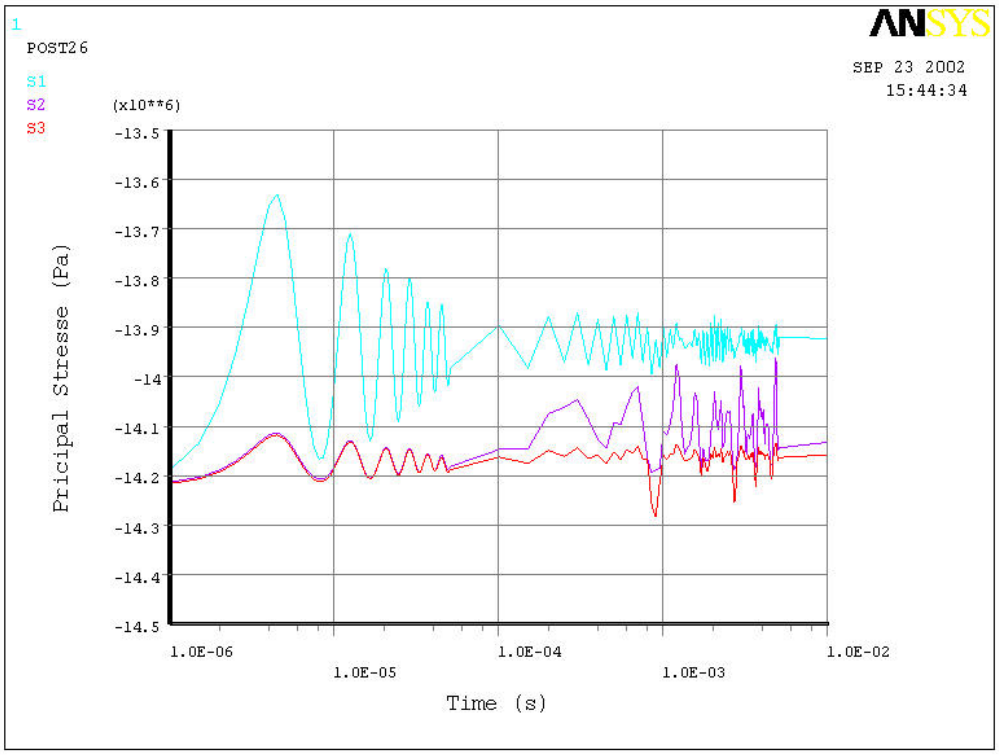

B: With damping

Figure 24: Elastic waves in graphite with and without material damping.

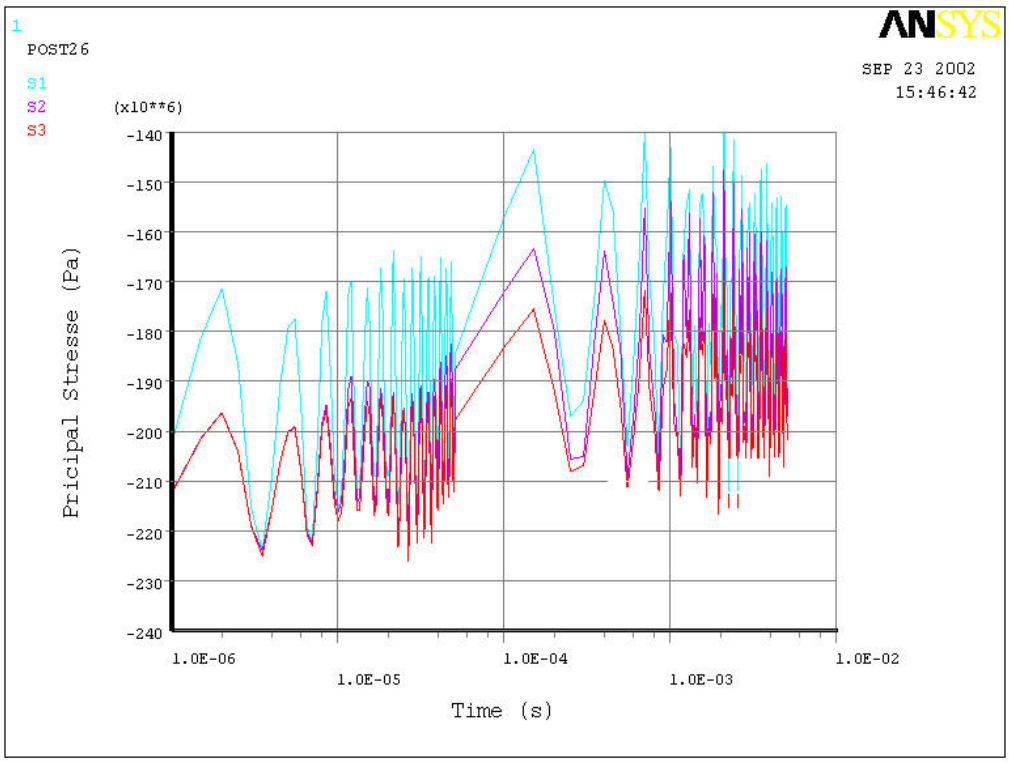

A: Without damping

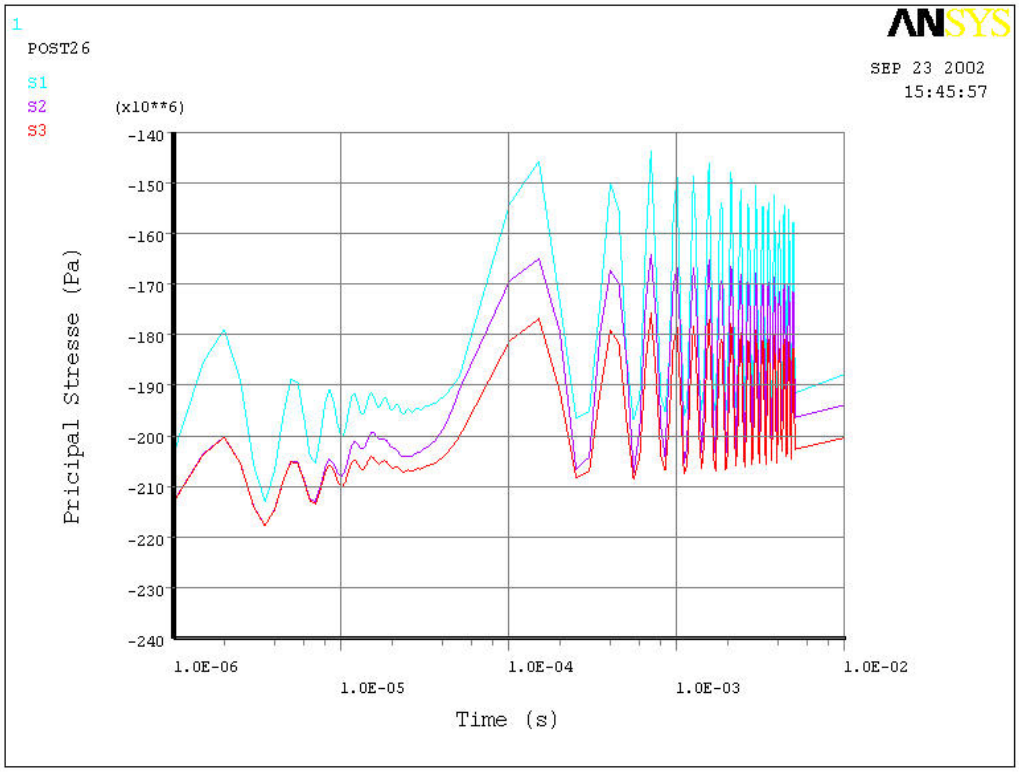

B: With damping

Figure 25: Elastic waves in aluminium with and without material damping.